HHS Public Access

Author manuscript

Cell Rep. Author manuscript; available in PMC 2024 April 18.

Published in final edited form as:

Cell Rep. 2024 February 27; 43(2): 113707. doi:10.1016/j.celrep.2024.113707.

H2A.Z histone variants facilitate HDACi-dependent removal of H3.3K27M mutant protein in paediatric high-grade glioma cells

Katarzyna B. Leszczynska[1,*], **Amanda Pereira de Freitas**[1], **Chinchu Jayaprakash**[1], **Monika Dzwigonska**[1], **Francisca N. L. Vitorino**[3], **Cynthia Horth**[4], **Kamil Wojnicki**[1], **Bartlomiej Gielniewski**[1], **Paulina Szadkowska**[1], **Beata Kaza**[1], **Javad Nazarian**[5,6], **Maciej K. Ciolkowski**[2], **Joanna Trubicka**[2], **Wieslawa Grajkowska**[2], **Benjamin A. Garcia**[3], **Jacek Majewski**[4], **Bozena Kaminska**[1], **Jakub Mieczkowski**[1,7,8,*]

[1]Laboratory of Molecular Neurobiology, Nencki Institute of Experimental Biology, Warsaw, Poland;

[2]Children's Memorial Health Institute, Warsaw, Poland;

[3]Department of Biochemistry and Molecular Biophysics, Washington University School of Medicine, St. Louis, MO, USA.

[4]Department of Human Genetics, McGill University, Montreal, Quebec, Canada;

[5]Center for Genetic Medicine Research, Children's National Hospital, Washington, DC, USA;

[6]Department of Pediatrics, University Children's Hospital Zürich, Zürich, Switzerland;

[7]3P-Medicine Laboratory, Medical University of Gdansk, Gdansk, Poland

[8]Lead contact

SUMMARY

Diffuse intrinsic pontine gliomas (DIPG) are deadly paediatric brain tumours, non-resectable due to brainstem localisation and diffusive growth. Over 80% of DIPGs harbour a mutation in histone 3 (H3.3 or H3.1) resulting in a lysine to methionine substitution (H3K27M). Patients with DIPG have a dismal prognosis with no effective therapy. We show that HDAC inhibitors lead to the significant reduction in the H3.3K27M protein (up to 80%) in multiple glioma cell lines. We discover that the SB939-mediated H3.3K27M loss is partially blocked by a lysosomal inhibitor, chloroquine. The H3.3K27M loss is facilitated by co-occurrence of H2A.Z, as evidenced by the knock-down of H2A.Z isoforms. ChIPseq analysis confirms the occupancy of H3.3K27M and H2A.Z at the same SB939-inducible genes. We discover a mechanism showing HDAC inhibition in DIPG leads to pharmacological modulation of the oncogenic H3.3K27M protein levels. These findings show possibility to directly target the H3.3K27M oncohistone.

[*]correspondence: jakubm@gumed.edu.pl, k.leszczynska@nencki.edu.pl.

AUTHORS CONTRIBUTIONS

KBL conceived, designed, performed, supervised experiments and interpreted the results; and wrote the manuscript. JM (Mieczkowski) conceived the project and secured the funding; conceived, designed or supervised the experiments; performed computational analyses and interpreted the results; wrote the manuscript. APDF, CJ, MD, FNLV, CH, KW, BG, PS, BK (Kaza), JN, BAG and JM (Majewski) performed the experiments. MKC, WG and JT provided pHGG biopsies from patients to derive cell lines and performed the molecular analysis of biopsies. BK (Kaminska) provided guidance on the project, infrastructure for the experiments and co-wrote the manuscript.

DECLARATION OF INTERESTS

JM is a cofounder and shareholder in Genegoggle. The remaining authors declare that they have no competing interests.

Keywords

H3.3K27M; H2A.Z; HDAC inhibitors; DIPG; paediatric high-grade gliomas

INTRODUCTION

In eukaryotes, the chromatin structure is organised through nucleosomes composed of genomic DNA wrapped around cores histones [1]. H2A, H2B, H3 and H4 are the four types of core histones, represented by 'canonical' replication-dependent histones, or replication-independent histone variants [2]. The presence of histone variants in nucleosomes plays a particular role in regulating the chromatin structure and gene expression, and, as it is in case of H2A.Z and H3.3 histone variants, may have opposing effects [3]. H2A.Z is concentrated at the promoters of inducible genes with low basal gene expression and is removed during transcription. [4,5]. Recent studies indicate that H2A.Z can even inhibit gene transcription [6]. Conversely, H3.3 is regarded as a marker of actively transcribed genes [7,8]. The presence of particular histone variants proves critical in certain diseases, and particularly, in tumorigenesis [9].

Paediatric high-grade gliomas (pHGGs) of the midline brain structures such as pons, thalamus and spinal cord are classified as H3K27-altered diffuse midline gliomas (DMG), due to the global loss of lysine 27 trimethylation (H3K27me3) and a corresponding increase in H3K27 acetylation (H3K27ac) [10–13]. In most cases, the H3K27 hypomethylation is caused by non-synonymous histone mutation resulting in a Lys27 (K27) to methionine (M) substitution mainly in H3.3, and to a lesser extent in H3.1/H3.2 histones (H3K27M). In paediatric diffuse intrinsic pontine gliomas (DIPGs), the mutated H3K27M histone variant is expressed in more than 80% of cases [10,11]. H3K27M directly binds Enhancer of Zeste Homolog 2 (EZH2), the methyltransferase unit of the Polycomb Repressive Complex 2 (PRC2) resulting in inhibition of EZH2 and the loss of H3K27me3. PRC2 can also be inhibited by overexpression of EZH Inhibitory Protein (EZHIP), which occurs in K27-altered DMGs that do not express the H3K27M oncohistone [10–12,14–17]. H3K27M-dependent loss of H3K27me3 leads to altered activities of specific gene promoters and consequent transcriptional changes including so called 'H3K27M signature genes', PRC2 target genes, BMI1, PI3K, and NOTCH pathways along with other genes involved in gliomas [10,18,19].

CRISPR and shRNA-mediated removal of H3K27M reverses its oncogenic function, restore the distribution of H3K27me3 and H3K27ac modifications at the chromatin and normalise the expression of genes affected by H3K27M [20,21]. However, currently there are no ways to eradicate this mutation from the tumours pharmacologically and efforts focus on targeting other epigenetic (epigenetic meaning alterations in histone post-translational modifications and/or DNA modifications) vulnerabilities of DMGs [22]. Promising results in pre-clinical studies have been achieved with histone deacetylase inhibitors (HDACi), e.g. panobinostat, which induced glioma cell death, impaired the growth of tumour xenografts [23]. Panobinostat also partially restored H3K27me3 levels in H3K27M DMG cells and reversed the expression of 'H3K27M signatures', although the mechanism behind this

indirect action of the drug is unclear [23–25]. Panobinostat as a single agent did not improve the patient outcome. however, treatments with other drugs, e.g. with proteasomal or transcriptional inhibitors showed promising effects encouraging clinical trials [26,27]. New therapeutics for children with DIPG are desperately needed as more than 90% of cases recur after radiotherapy and die within 9–12 months after diagnosis [28].

We show that HDAC inhibitors (pracinostat/SB939, panobinostat, vorinostat and entinostat) lead to a significant decrease in H3.3K27M protein levels, without affecting the *H3F3A* mRNA expression. The genome-wide analysis in SB939-treated cells confirmed the effects on H3K27M occupancy and dependent genes. We demonstrate that SB939-dependent loss of H3.3K27M is impaired by treatment with chloroquine, the inhibitor of autophagosome/lysosomal degradation and DNA intercalating agent. The loss of H3.3K27M protein upon SB939 treatment is facilitated by co-occurrence of H2A.Z histone variants. Altogether, we show mechanism of action of HDACi, which may pave ways to therapeutic approaches in these deadly paediatric tumours.

RESULTS

We have performed a cell viability screen with selected drugs targeting epigenetic modifiers to search for compounds that could be efficient in targeting epigenetically-vulnerable pHGG cells expressing H3K27M. We initially used three patients derived human primary DMG cell lines (SF8628, SF7761 and WG27) (Figure 1A and Supplementary Table 1). Panobinostat and GSK-J4 were included as a reference, as these previously showed effectiveness against pHGGs (Figure 1A) [23,29]. Several of the drug candidates reduced DMG cell viability at 10 μM concentrations (JIB-04, Methylstat, UNC0638, UNC0642, SB939/pracinostat) and were therefore further tested in a panel of cell lines and at a range of concentrations (Figure 1B and Supplementary Figure 1A–E). We found that all the shortlisted candidate drugs significantly decreased cell viability at sub-micromolar concentrations, but SB939, which is an HDACi, was less efficient against the WG27 cells, which expressed lower amounts of the mutated histone H3K27M when compared to other cell lines (Figure 1A–B and Supplementary Figure 1F–G). The effect of SB939 has not been previously characterised in H3K27M$^+$ pHGGs; here we found that it induced apoptosis and decreased cell proliferation in these cells (Supplementary Figure 1H–I). We then investigated whether the presence of H3.3K27M mutation confers increased sensitivity towards SB939. We examined cell viability in six additional patient-derived pHGG cell cultures with different H3.3K27 status (Figure 1C and Supplementary Table 1). We observed that mutant H3.3K27M cells were significantly more sensitive to SB939 treatment compared to cells with wild type H3.3 wild type: approximately 50% of H3.3K27M$^+$ cells survived 72-hour treatment with 1 μM SB939, while more than 50% of H3.3 wild type cells survived 72-hour treatment with 10 μM SB939, 2-way ANOVA *P=0.019,* (Figure 1C). To further verify this observation, we used previously published isogenic cells, in which the H3.3K27M mutation was eliminated with CRISPR technology from the parental cell line (Supplementary Table 1) [30,31]. We observed a higher sensitivity to the drug at lower concentrations (two-way ANOVA *P=0.005*) when the H3.3K27M mutant was present only in one out of three tested cell lines (HSJ019) (Figure 1D–E and Supplementary Figure 1J). However, in all three cell lines (even in cells with deleted H3.3K27M by CRISPR), 50% cell killing occurred at

concentrations below 1 μM SB939 (Figure 1D–E and Supplementary Figure 1J). We also compared sensitivity of normal human astrocytes (NHA), which do not contain the H3 mutation, and these cells required higher SB939 concentrations (above 1 μM) to achieve 50% cell kill (Supplementary Figure 1K). Together, these data suggested that pHGG cells that have the H3.3K27M mutation (or had it originally before gene deletion) are more sensitive to SB939 compared to H3 wild type pHGG cells. However, since the deletion of the mutation in the isogenic system did not conclusively decrease the sensitivity towards SB939 in all cell lines (Figure 1D–F), this suggests that other factors are also involved in the sensitivity to HDACi, which likely evolved during the growth of H3K27M^{+} pHGGs tumours.

Importantly, we observed that the treatment with SB939 caused a marked decrease in the levels of the mutated histone (Figure 1F). The H3.3K27M antibody used was of a very high quality and specificity towards the mutated histone variant (Supplementary Figure 1L). Only the treatment with SB939 caused the decrease in H3.3K27M levels in comparison to other tested compounds (Figure 1G).

Because pharmacological reduction of the H3.3K27M protein is desirable, we have investigated the molecular underpinning of this effect. We found that the SB939-mediated decrease of H3.3K27M levels was dose-dependent (Figure 1H and Supplementary Figure 1M) and consistent in all tested cell lines, including cells grown as adherent monolayers in FBS-containing medium (SF8628, WG30), cells grown as adherent monolayers in the Neurocult medium without FBS (DIPGXIII), as well as cells cultured as spheres (7316–195, 7316–1763 and SF7761) (Figure 1G–J and Supplementary Figure 2A–B). In addition, we tested two cell lines where the K27M substitution occurs in H3.1 histone variant (CNHDMG-1008 and CNHDMG-1277 cells), and, similarly as for H3.3K27M, we observed reduction of the H3.1K27M in response to SB939 (Supplementary Figure 2C–D). We also tested alternative lysis method with acid histone extraction and found a similar decrease in the H3.3K27M levels after SB939 exposure (Supplementary Figure 2E). We then tested the kinetics of H3.3K27M decrease in response to SB939 in two different cell lines and found that downregulation of H3.3K27M was significant as early as one hour after the treatment with SB939, with the strongest decrease observed between 6 and 24 hours of treatment (Figure 1K–L and Supplementary Figure 2F–G). The levels of H3.3K27M recovered around 48 hours after the treatment. The effect of SB939 treatment on the upregulation of the histone 3 acetylation was prolonged up to 72 hours, as shown by the total H3 acetylation and H3K27ac levels (Figure 1K–L and Supplementary Figure 2F–G).

We then examined whether other HDACi could exert a similar effect on H3.3K27M. We treated SF7761 spheres for 24 hours with SB939, panobinostat, vorinostat and entinostat and examined the levels of H3.3K27M. We found a decrease in H3.3K27M levels in response to all the inhibitors tested, although the effect was weaker in vorinostat and entinostat treated cells, which also coincided with a smaller effect of these drugs on upregulation of H3 and H4 acetylation (Figure 1M). A previous study demonstrated that shRNAs towards HDAC1 and HDAC2 were efficient as single treatments in impairing the viability of DIPG cells [23]. We therefore investigated whether silencing of these HDACs would result in a decrease in H3.3K27M levels. We transfected SF8628 cells with siRNA against HDAC1, HDAC2

or both. We did observe a mild decrease in the H3.3K27M levels, when the HDAC1 and HDAC2 were knocked-down together and this effect was more pronounced when we carried out a double knock-down procedure on two consecutive days (Supplementary Figure 2H–K). In addition, the effect of HDAC1/2 knock-down on histone acetylation levels was very moderate in comparison to the one seen with HDAC inhibitors, suggesting that pan-HDAC inhibition and a very robust histone hyper-acetylation might be required in order to facilitate the repression of H3.3K27M (as seen for HDACi treatment) (Figure 1M and Supplementary Figure 2H–K).

Next, we verified whether the H3.3K27M protein loss after SB939 treatment can globally affect the H3.3K27M occupancy at the chromatin. We performed a ChIP-seq analysis in SF7761 and DIPGXIII cells for the H3.3K27M and H3.3 total enrichment at the chromatin after 16 hours of treatment with SB939 (the time which corresponds to the most robust reduction of H3.3K27M). As expected, SB939 caused a global loss of the H3.3K27M occupancy at the chromatin. In contrast, the levels of the total H3.3 remained unchanged or even slightly increased after SB939 treatment (Figure 2A–B).

The presence of H3K27M mutation was previously shown to drive specific transcriptomic programs, often referred as ‘H3K27M signatures’ [10,12]. Therefore, we explored gene expression changes induced by SB939 treatment using RNA sequencing. We hypothesised that the loss of H3K27M in response to SB939 could reverse these ‘signatures’. The PCA analysis showed a clear separation of samples based on the cell lines and SB939 treatment (Supplementary Figure 3A). As we found that SB939-triggered gene expression changes correlated between the two cell lines tested (Spearman’s correlation=0.68 and Pearson’s correlation=0.69), we continued further analyses on data integrated from these two cell lines (Supplementary Figure 3B). We identified 2,148 upregulated and 1,557 downregulated genes in SB939-treated cells (Supplementary Figure 3C). Interestingly, the genes that were up-regulated after SB939 treatment had a very low basal expression in control cells (DMSO-treated) in comparison to the ones that became downregulated or to the average expression of all the genes (Figure 2C). This observation suggests that SB939 “unlocked” the genes with the low constitutive expression, while diminishing the expression of highly expressed genes. The loss of H3.3K27M from the chromatin occurred at both up- and down-regulated genes (Figure 2D–E). However, for the up-regulated genes the H3.3K27M occupancy was the highest at the ones with the smallest constitutive expression in control cells (Figure 2D and Supplementary Figure 3D). This dependency was not seen at the genes downregulated after SB939 treatment (Figure 2E and Supplementary Figure 3E).

To explore functionality of these genes, we performed a Gene Ontology (GO) analysis on SB939 down- and up-regulated genes, and we identified multiple pathways enriched in both groups, respectively (Supplementary Figure 3F–G). We have also compared the gene expression induced here with SB939 and in the publicly available RNAseq datasets induced with panobinostat treatment. We found a significant correlation between the gene expression changes induced by SB939 and by panobinostat in DIPGXIII and BT245 cells (Supplementary Figure 3H).

We then investigated the H3.3K27M enrichment at genes that became up or downregulated and which enrichment was lost after SB939 treatment. We detected 6,160 enriched H3.3K27M regions common for the two cells lines in DMSO-treated samples, of which 4,403 disappeared after SB939 treatment. After annotation to the coding genes, we found that these enrichments disappeared at 305 upregulated and 276 downregulated genes in SB939 treated cells (Figure 2F). However, considering that more genes were upregulated (2,148) than downregulated (1,557) (Supplementary Figure 3C), the loss of H3K27M enriched sites was more pronounced and statistically significant only in downregulated genes. In addition, we compared the enrichment of H3.3K27M on these 305 up- and 276 downregulated genes identified in this study in other datasets withH3.3K27M ChIPseq data in pHGG cells. H3.3K27M was consistently enriched at these genes in comparison to all the genes (Supplementary Figure 4A–B). Moreover, in public transcriptomic datasets from panobinostat or entinostat treated pHGG cells, we observed a similar pattern of expression of these 305 up and 276 downregulated genes (Supplementary Figure 4C). The H3.3K27M KO led to smaller expression changes of these genes (Supplementary Figure 4D). The GO enrichment analysis of these down-regulated genes with the H3.3K27M loss identified numerous pathways, including neuron projection development, plasma membrane bounded cell projection morphogenesis, axon guidanceetc (Supplementary Figure 4E). Those pathways have been previously linked to the H3K27M oncohistone in gliomas [12]. Interrogation of our data with the known “H3K27M signatures” encompassing 143 genes previously reported as upregulated in H3.3K27M-expressing pHGGs revealed that out of the 143 H3.3K27M-dependent genes, 26 were down-regulated in SB939-treated samples in both cell lines, including the synaptic adhesion molecule neuroligin-3 (*NLGN3*), which promotes pHGG growth (Fisher’s exact Pv=3e-04) (Figure 2G–H and Supplementary Figure 4F, the heatmap for all 143 genes is in the Supplementary Figure 4G) [12,32,33]. These data show that SB939 treatment, which leads to the downregulation of H3.3K27M, also leads to the loss of a group of genes previously reported as H3K27M-dependent [12]. However, it is important to stress that the effect of HDAC inhibition on gene expression might be stronger than the effect of the loss of H3.3K27M during HDAC inhibition, which could explain why not all 143 H3.3K27M-dependent genes were regulated in the same way after HDACi treatment (Figure 2G and Supplementary Figure 4F).

Next, we investigated the mechanism of the H3.3K27M loss in response to SB939. The qPCR analysis showed increased expression of *H3F3A* and *H3F3B* genes in response to SB939 treatment (Figure 3A–B). Similar results were observed in RNAseq data from cells treated with SB939 (Supplementary Figure 5A) as well as in previously published RNAseq data sets for cell lines treated with panobinostat (Supplementary Figure 5B–C). Importantly, analysis of the RNAseq data for the ratio of reads with the mutated H3.3M27 (ATG) versus the wild type H3.3K27 (AAG) sequence showed that 16 hours after SB939 treatment this ratio was not affected in the two tested cell lines (Supplementary Figure 5D). A gradual increase in the *H3F3A* mRNA after SB939 with time that persistent up to 72 hours (Figure 3C). Expression of the *H3F3B* mRNA increased initially, but then declined from 16 hours of treatment (Figure 3D). Furthermore, the ratio of reads with the mutated H3.3M27 (ATG) versus the wild type H3.3K27 (AAG) sequence remained constant throughout the whole time-course of SB939 treatment, altogether suggesting that the initial loss of the H3.3K27M

protein does not occur at the mRNA level (Figure 3E). The recovery of H3.3K27M at 72 hours after SB939 could result from gradual increase of the *H3F3A* mRNA (both wild type and mutated). The Western blotting also showed the gradual accumulation of the total H3.3 proteins (Figure 3D, Figure 1K–L and Supplementary Figure 2F–G). Importantly, some of the genes noted earlier as co-repressed together with the loss of H3.3K27M after 16 hours of SB939 treatment (Figure 2G) recovered their expression with the restoration of the H3.3K27M protein at later time points (Figure 3G). Interestingly, while the expression of H3.3 chaperones *HIRA* and *DAXX* was repressed with time after HDAC inhibition, expression of *ATRX* followed the expression pattern of H3.3K27M with a recovery at 48–72 hours of treatment (Figure 3H–J), which could play a role in the restoration of H3.3K27M into the nucleosomes.

These data suggest that the reduction of H3.3K27M in response to SB939 treatment occurs likely at the protein level and not as a result of decreased mRNA expression. To test this hypothesis, we overexpressed the construct coding for N-terminally Flag-tagged H3.3K27M (Flag-H3.3K27M) in the LN18 glioma cells. Western blotting showed that the signal from the Flag-H3.3K27M band decreased in response to SB939 treatment with both Flag and H3.3K27M antibodies, while the mRNA expression of the construct remained unchanged upon the treatment (Figure 4A–B). To determine whether the wild type H3.3 is similarly affected by SB939 treatment as the mutated histone, we overexpressed the Flag-H3.3K27M and Flag-H3.3WT, in parallel. Only downregulation of the mutated Flag-H3.3K27M was apparent, but not the wild-type Flag-H3.3 or endogenous H3.3 (Figure 4C). This result suggests that SB939 treatment specifically reduces the H3.3K27M protein in glioma cells. Finally, we have carried out a mass spectrometry analysis of the mutated and wild type peptides in SF7761 and DIPGXIII cells treated for 16 hours with SB939. We have observed a significant drop in the ratio of mutated to wild type H3.3_27–40 peptide after SB939 treatment (Figure 4D). At the same time, the H3 acetylation increased with time of SB939 treatment, as shown for the H3K27ac_27–40 peptide (Figure 4E).

Subsequently, we examined which of two major protein degradation pathways could be responsible for the potential reduction of H3.3K27M levels upon SB939 treatment. The treatment with a proteasomal inhibitor, MG-132, had no significant effect on the levels of the mutated histone in SB939-treated cells (Figure 4F). MG-132 stabilised the expression of HIF-1α protein, which is targeted for degradation via E3 ubiquitin ligase VHL and proteasome, confirming that the proteasome degradation pathway has been inhibited (Figure 4F). We then tested autophagosome/lysosomal pathway for the potential degradation system of H3.3K27M. Interestingly, the addition of chloroquine (CQ), which impairs lysosomal degradation by increasing the pH of lysosomes, partially restored the levels of H3.3K27M decreased by SB939 (Figure 4G).

Previous reports have shown that fragments of chromatin can be cleared via lysosomal degradation under certain circumstances, however these studies did not investigate the effect of HDAC inhibition on this process [34,35]. We examined the cellular localisation of endogenous H3.3K27M via immunofluorescent staining and asked how it changed in response to SB939 treatment and after the rescue with CQ. The nuclear intensity of H3.3K27M was significantly reduced upon the treatment with SB939 and rescue of the

nuclear H3.3K27M was visible when CQ was present during the SB939 treatment (Figure 4H–I). In addition, we observed that in each condition, a fraction of cells had extracellular vesicles present in the cytoplasm that contained DNA (stained with DAPI) and H3.3K27M (as indicated in Figure 4H with arrows in the representative picture for SB939+CQ). We determined the percentage of cells in each condition with visible cytoplasmic vesicles. While cells with these vesicles were the least abundant in the SB939-treated group, these were significantly increased when the CQ was present (Figure 4J). This result suggests that CQ impairs the clearance of the chromatin (and H3.3K27M) in these vesicles exported extranuclearly. However, the nuclear rescue of H3.3K27M was also visible in SB939+CQ treated samples (Figure 4I), implying that some CQ-dependent direct or indirect mechanisms of H3.3K27M downregulation in the nuclei also existed upon SB939 treatment.

While our data supported the notion that chromatin fragments containing H3.3K27M were at least partially cleared via lysosomes, it was difficult to explain why this process was so rapid and temporary, and whether this would be the only clearance pathway of the mutated histone. Therefore, we investigated more thoroughly the events coinciding with the H3.3K27 loss triggered by SB939 treatment. As expected for the HDACi, the treatment with SB939 caused an immediate and significant increase in the acetylation of numerous histones, including H3, H4, but also H2A.Z histone variant (Figure 5A). Such increased histone acetylation could potentially cause destabilisation of nucleosomes and chromatin relaxation [36]. Previous studies showed that incorporation of the H2A.Z and H3.3 histone variants in the same nucleosomes made them more unstable than the presence of canonical H2A and H3 histone variants, although the significance of H2A.Z histone variant in the nucleosome stability in H3.3K27M-expressing DIPG cells has not been investigated to date [37,38]. As our antibody against H2A.Z does not distinguish between H2A.Z.1 (encoded by *H2AFZ*) and H2A.Z.2 (encoded by *H2AFV*) isoforms, we have investigated the expression of both these genes upon SB939 treatment in various cell lines using qPCR or in RNAseq datasets from HDACi treated cells. We have found that expression of the more abundant isoform, *H2AFZ*, was decreased in response to HDACi in majority of the analysed datasets, while *H2AFV* did not significantly change or was even moderately increased in some cells (Supplementary Figure 6A–E). This change was even more clear when we examined expression of *H2AFZ* and *H2AFV* in a time-course treatment with SB939 (Supplementary Figure 7A–B). This result could potentially explain the relatively stable overall levels of the H2A.Z protein detected with the pan-H2A.Z antibody after the SB939 treatment that also gradually increased with time in SB939 treated cells (Figure 5A and Supplementary Figure 7C–H).

We assessed the H2A.Z occupancy at the chromatin and in the context of gene expression by performing the H2A.Z ChIPseq in SF7761 and DIPGXIII cells treated with SB939. The ChIPseq conditions for H2A.Z were matching the ones showed earlier for H3.3 and H3.3K27M in Figure 2. In one of the cell lines (SF7761) SB939 treatment caused average H2A.Z loss in the TSS proximal regions in all the genes, but not in DIPGXIII cells (Supplementary Figure 8A). However, a more striking difference in the H2A.Z occupancy in both cell lines was apparent, when up- and down-regulated genes upon SB939 treatment were analysed separately. The highest H2A.Z occupancy was observed at the genes with the lowest expression in DMSO samples and that then became up-regulated by SB939 (Figure

5B and Supplementary Figure 8B). Moreover, this was more apparent, when we compared H2A.Z occupancy at all genes (black line), up-regulated genes (red line) and up-regulated genes with H3.3K27M loss (blue line) (Figure 5C/top row and Supplementary Figure 8C/top row). The genes with the highest loss of H2A.Z occupancy where the ones that also lost the H3.3K27M occupancy and became up-regulated by SB939 treatment (Figure 5C/middle row panel and Supplementary Figure 8C top/middle rows; bottom row with H3.3 WT is shown for the comparison).

The presented data suggest that the co-occurrence of both H3.3K27M and H2A.Z histone variants in close proximity at actively transcribed genes could facilitate their loss, particularly in the situation of increased histone acetylation during HDAC inhibition. Perhaps the presence of H2A.Z promotes the total loss of H3.3K27M in DIPG cells as was shown with Western blotting. To verify this hypothesis, we depleted H2A.Z levels in cells with siRNA and investigated the loss of H3.3K27M after SB939 treatment. SF8628 cells were double transfected with two different siRNAs targeting either *H2AFZ* or *H2AFV* expression to ensure a prolonged knock-down of H2A.Z. Transfected cells were treated with SB939 for 24 hours and we performed qPCR and western blotting analyses. The specificity and effectiveness of silencing was confirmed with qPCR primers detecting both H2A.Z isoforms (Figure 5E). Importantly, the knock-down of either *H2AFZ* or *H2AFV* genes consistently impaired the reduction of total H3.3K27M levels upon the SB939 treatment as shown by Western blotting (Figure 5F). Similar results were obtained with another DMG cell line (WG32) (Supplementary Figure 8E–F). However, we did not see any difference in rescuing the cell viability with H2A.Z knock-down in SB939-treated cells (Supplementary Figure 9A–B), potentially due to the fact that H3.3K27M rescue was only partial. Altogether, the presented data support the conclusion that HDAC inhibition promotes the loss of H3.3K27M, particularly in the presence of H2A.Z histone variants (Figure 5G).

DISCUSSION

DIPG childhood gliomas expressing the H3.3K27M oncohistone have the worst prognosis with no curative therapy available. In this study, we demonstrate that pan-HDAC inhibition leads to a significant decrease in the H3.3K27M protein levels in a number of H3.3K27M$^+$ cells. SB939-dependent decrease of H3.3K27M is very rapid and accompanied by an immediate increase in histone acetylation. We show that co-occurrence of H2A.Z and H3.3K27M at the same genomic locations pre-disposes cells to the HDACi-dependent loss of H3.3K27M, particularly at the genes which will become up-regulated upon SB939 treatment. Depletion of H2A.Z isoforms from H3.3K27M$^+$ DIPG cells significantly impairs the SB939-dependent loss of H3.3K27M, emphasising the role of the nucleosome components in the stability of the H3.3K27M protein. We also show that SB939-dependent loss of H3.3K27M is partially blocked with chloroquine, acting most likely through the inhibition of lysosomal degradation pathway.

Intriguingly, HDAC inhibition with SB939 leads to a preferable loss of the H3.3K27M oncohistone, but not the wild type H3.3 histone variant. This reduction of the histone H3.3K27M level is not due to decrease of transcription. We demonstrate that both *H3F3A* and *H3F3B* mRNA are elevated in response to HDAC inhibition and the total H3.3

protein levels accumulate with time. The previously reported mass spectrometry analysis showed that mutated H3.3K27M constitutes only between 3 to 17% of the total H3 protein levels, which could explain why the total H3.3 does not decrease in our data, especially if the *H3F3A* and *H3F3B* mRNA remain constant or are slightly upregulated after prolonged SB939 treatment [11]. We show that SB939 triggers cellular mechanisms leading specifically to the loss of H3.3K27M, while sparing the remaining wild type H3 histone pool.

We present two potential mechanisms responsible for selective downregulation of H3.3K27M protein. Out of two tested inhibitors of protein degradation pathways, chloroquine partially blocked the loss of H3.3K27M induced by SB939 treatment. It is not entirely clear how chloroquine impairs the SB939-mediated loss of H3.3K27M protein levels as this compound has multiple actions besides being the lysosomal/autophagosome inhibitor. Blockade of the lysosomal turnover of chromatin fragments after SB939 treatments by chloroquine is a plausible explanation for the H3.3K27M loss. This is in line with previous studies showing that H3 can be turned over via lysosomes in the autophagy process, however to date this has not been investigated in the context of HDAC inhibition [34,35]. In addition, the lysosomal degradation of H3.3K27M can offer only a partial mechanism of the H3.3K27M loss during HDACi treatment, as our data equally suggests that chloroquine already restores the H3.3K27M levels at the nuclear level. Chloroquine has been known for its DNA-intercalating properties, affecting DNA replication and RNA synthesis [39]. One could speculate that chromatin is stabilised by CQ intercalation and disassembly of nucleosomes is impaired, resulting in a weaker H3.3K27M degradation. Our findings suggest a potential dynamic interplay between HDAC inhibition, histone chaperones (*ATRX, HIRA*, and *DAXX*), and the loss and recovery of H3.3K27M containing nucleosomes. Especially since their connection with HDAC has already been reported [40]. Nevertheless, this mechanism needs a thorough future investigation.

Histone variants H2A.Z and H3.3, are frequently placed in the same nucleosomes and cooperate to regulate transcription [41]. As H2A.Z can be an oncogenic driver, we explored the role of H2A.Z in DIPG cells after HDAC inhibition [42,43]. We show that many of H2A.Z and H3.3K27M ChIP-seq peaks overlap with each other in DIPG cells at genes with a low constitutive expression. Additionally, both peaks are lost after HDAC inhibition at upregulated genes. The function of H2A.Z in H3.3K27M^{+} tumours and in the context of sharing the nucleosomes with H3.3K27M has not been investigated yet. The unstable H3.3-H2A.Z nucleosomes might be even more affected when H3.3 is substituted with the H3.3K27M oncohistone. However, it is equally possible that the presence of H2A.Z, and particularly its hyperacetylated form, might recruit some additional proteins, like RNA polymerase II and other partners that will additionally alter gene expression or induce turnover of H3.3K27M containing nucleosomes [42]. Future studies will focus on deciphering the role of H2A.Z in the H3.3K27M stability and turnover.

In summary, this is a first demonstration that decreasing the levels of the detrimental H3.3K27M oncohistone can be achieved pharmacologically with HDAC inhibitors. While this discovery does not offer an immediate therapeutic solution to improve the outcome of DMG patients, these results open some alternative pathways to target H3.3K27M. The

ultimate future goal is to explore the potential of such mechanisms in H3.3K27M-driven tumorigenesis.

LIMITATIONS OF THE STUDY

While this work shows the exciting possibility to remove the mutated H3K27M oncohistone, the precise mechanism of this process is not fully elucidated. Characterisation of the molecular machinery involved in removing the H3K27M in response to HDAC inhibition/histone acetylation is needed to fully explore the translational potential of this discovery. Conducting a detailed investigation of nucleosomes that contain HA.Z, H3.3, H3.3K27M, or a combination of these histones, with the assistance of histone chaperones, may offer valuable biophysical insights into stability, degradation mechanisms, and the dynamic regulation of chromatin structure in response to HDACi.

STAR★Methods

Resource availability

Lead contact—Further information and requests for resources and reagents should be directed to and will be fulfilled by the lead contact, Jakub Mieczkowski (jakubm@gumed.edu.pl).

Materials availability—pcDNA4/TO-Flag-H3.3K27M plasmid will be shared upon request. WG27, WG30, WG32 cells will be shared upon request under MTA completion.

Data and code availability

- The RNA-seq data, and ChIP-seq data for H3.3, H3.3K27M and H2A.Z histone variants in DIPGXIII and SF7761 cell lines generated in this paper is available at NCBI GEO under accession code GSE232283. Mass spec data generated in this paper has been deposited at MassIVE database under the accession number MSV000093052. All other relevant data supporting the key findings of this study are available within the article and its Supplemental information files.
- The custom R code used to analyze the generated data is attached as a supplementary item to the paper.
- Any additional information required to reanalyse the data reported in this work paper is available from the lead contact upon request.

Experimental model and study participant details

Cell culture models—SF8628 and SF7761 cells were a kind gift from Dr Rintaro Hashizume [29,45,46]. SF8628 cells were cultured as adherent cells in DMEM/F12 media (Gibco, Cat# 11330–032) supplemented with 10% fetal bovine serum (FBS), 1% (v/v) and MEM non-essential amino acids. SF7761 cells were grown as spheres in tumor stem medium base (containing 50% DMEM/F-12 and 50% Neurobasal A (v/v)) supplemented with 1% (v/v) HEPES, 1% (v/v), 1% (v/v) MEM Sodium Pyruvate Solution 100mM, 1% (v/v) MEM non-essential amino acids, % (v/v) GlutaMAX, 1% (v/v) Antibiotic-

Antimycotic, 2% (v/v) B27 Supplement w/o Vitamin A, rhEGF (20 ng/ml), bFGF (20 ng/ml), PDGF-AB (20 ng/ml) and 2.5 μg/ml Heparin. BT245, SU-DIPG-XIII (referred in the text as DIPGXIII) and HSJ019 were a kind gift from Dr Nada Jabado (McGill University) and were cultured as adherent cells on poly-L-Ornithine and Laminin coated flasks in medium containing Neurocult NS-A Basal Medium and Supplement, rhEGF (20 ng/ml), bFGF (10 ng/ml) and Heparin (2.5 μg/ml) [20,30,31]. 7316–1769, 7316–1763, 7316–195, 7316–913, 7316–1746 and 7316–85 pHGG cells were obtained from the Children's Brain Tumor Tissue Consortium (CBTTC, via The Children's Hospital of Philadelphia (CHOP)) and were cultured as spheres in DMEM/F12, 1% (v/v) GlutaMAX, 2% (v/v) B27 Supplement w/o Vitamin A, 1% (v/v) N2 supplement, rhEGF (20 ng/ml), bFGF (20 ng/ml) and 2.5 μg/ml Heparin. CNHDMG-1008 and CNHDMG-1277 DMG cells expressing H3.1K27M were cultured in the same conditions as SF7761 cells described above [47–50]. LN18, LN229 and U-251 were cultured in DMEM media supplemented with 10% (v/v) FBS (from ATCC). All media above were additionally supplemented with penicillin and streptomycin antibiotics. All cells were maintained at 37 °C in humidified incubators supplied with 5% CO_2.

Human samples—The use of tumor biopsies was approved by the Research Ethics Committee at CMHI in Warsaw, Poland, and informed consents were obtained from all subjects. WG27, WG30 and WG32 cells were derived from pHGG patient biopsies collected at the Children's Memorial Health Institute (CMHI) in Warsaw as described previously [51]. Biopsies were placed in DMEM/F12 medium and transported on ice from the hospital. Tissues were dissected mechanically with a scalpel on a Petri dish in 0.5 ml of DMEM/F12 medium until homogenous tissue suspension was achieved. After filtering through 100- and 40-micron cell strainers cells were centrifuged and washed with fresh DMEM/F-12. Cells were resuspended in DMEM/F-12 medium supplemented with 10% (v/v) foetal bovine serum and 1% (v/v) antibiotic-antimycotic and cultured as adherent cells. Cell proliferation was monitored. Expression of the H3.3K27M mutation in obtained well-proliferating cultures was determined with Western blotting. The gender identity and age of each human subject from whom the DMG biopsy was obtained to derive primary cell cultures is as follows: WG27 (female, 6 years), WG30 (male, 4 years), WG32 (male, 15 years).

Method details

Plasmid and siRNA transfection—pcDNA4/TO-Flag-H3.3 was a gift from Bing Zhu (Addgene plasmid #47980; http://n2t.net/addgene:47980; RRID:Addgene_47980) [44]. The plasmid expressing Flag-H3.3K27M was generated by site-directed mutagenesis of pcDNA4/TO-Flag-H3.3 plasmid using primers: F: 5'-GAGTGCGCCCTCTACTGG-3' and R: 5'- ATGCGAGCGGCTTTTGTAG-3'. Successful mutagenesis was confirmed by sequencing at Genomed S.A. (Warsaw, Poland). Plasmid transfections into LN18 cells were performed with jetPRIME transfection reagent (114–07, PolyPlus), according to manufacturer's instructions. siRNA transfections in adherent SF8628 and WG32 cells were performed with DharmaFECT 1 transfection reagent (Dharmacon) according to manufacturer's protocol using the siRNA duplexes listed in the KRT.

Western blotting—Cells were washed in PBS and lysed in SDS lysis buffer (10 mM Tris-Cl, pH 7.5, 0.1 mM EDTA, 0.1 mM EGTA, 0.5% SDS, 0.1 mM β-mercaptoethanol, protease/phosphatase inhibitors), followed by sonication and centrifugation. Lysates with equal amount of proteins were subjected to SDS-PAGE and western blotting. The primary antibodies used are listed in the Key resources table. An enhanced chemiluminescence detection system (ECL) and Chemidoc (BioRad) were used to develop the signal from HRP-conjugated secondary antibodies.

For acid histone extraction assay, cells were resuspended in Triton Extraction Buffer (PBS containing 0.5% Triton X 100 (v/v) and protease inhibitors) at a cell density of 107 cells per ml, lysed on ice for 10 minutes, and centrifuged (2000 rpm, 10 min, 4 °C). Subsequently, cells were washed in fresh buffer and centrifuged again. Acid extraction of histones was carried out over night at 4 °C in 0.2N HCl at cell density of 4×107 per ml. After centrifugation, protein concentration in the supernatant containing extracted histones was determined with Bradford assay.

qPCR—Glioma cells were treated accordingly and total RNA was isolated with RNeasy Plus Kit (Qiagen) according to manufacturer's instructions; RNA concentrations and purity were assessed with NanoDrop 2000 (Thermo Fisher Scientific). Equal amounts of total RNA per each condition were used to make cDNA with SuperScript™ III Reverse Transcriptase kit (Invitrogen) and oligo-dT primers. PCR reactions with technical triplicates were performed with 2× Fast SYBR GREEN PCR Master Mix (Applied Biosystems) using QuantStudio 12K Flex equipment (Applied Biosystems, Life Technologies). The qPCR primer sequences are listed in the Supplementary Table 3.

Cell viability and cell proliferation assays—For cell viability, MTT assay was performed. 5×10^3 cells were seeded onto 96-well plates and cells that were cultured as spheres were supplemented with 5% FBS to attach for the time of the assay, as previously indicated [23]. Next day, the drug dilutions were added in technical triplicates. After 72 hours, the MTT solution (0.5 mg/mL; Sigma-Aldrich) was added and after 1 hour of incubation at 37 °C was replaced with 100 μl of DMSO to dissolve water-insoluble dark blue formazan crystals present in the attached cells. Optical densities were measured at 570 nm and 620 nm using a scanning multi-well spectrophotometer. For cell proliferation, cells were seeded at density of 5×10^3 per well in 96-well plates. Cells were treated with dilutions of SB939 for 24 or 48 hours and cell proliferation was assessed using ELISA BrdU kit (Roche Diagnostics GmbH), according to manufacturer's protocol.

Immunofluorescence—SF8628 cells were seeded on glass coverslips in 24-well plates at density of 2×104 cells per well, and the next day 1 hour treatment with SB939 in the presence or absence of chloroquine was performed. Cells were washed with PBS, fixed for 10 minutes with 4% PFA, followed by a triple wash with PBS. This was followed by 10-minute permeabilization with ice-cold 100% methanol and wash in PBST. After 1 hour blocking (3% donkey serum, 1% BSA, 0.3% Triton X-100, PBS) the H3.3K27M antibody (1:500, 61803, Active Motif) diluted in a blocking solution was added and incubated for 1 hour. This was followed by a triple wash in PBST and an hour incubation with a secondary donkey anti-rabbit antibody conjugated with Alexa Fluor-555 (1:2000, A31572, Invitrogen).

Coverslips were washed 3x with PBST and once with distilled water, followed by mounting with Vectashield mounting solution with DAPI (Vector Laboratories).

Histone levels analysis by nano-LC-MS—SF7761 or DIPGXIII cells were treated for 16 hours with 1 μM SB939 or DMSO and 4 million cells from each condition were collected and frozen at −80°C. Thawed pellets were lysed in nuclear isolation buffer (15 mM Tris pH 7.5, 60 mM KCl, 15 mM NaCl, 5 mM $MgCl_2$, 1 mM $CaCl_2$, 250 mM sucrose, 10 mM sodium butyrate, 0.1% (v/v) beta-mercaptoethanol, commercial phosphatase and protease inhibitor cocktail tablets) containing 0.3% NP-40 alternative on ice for 5 min. Nuclei were subsequently washed twice in the same buffer without NP-40, and pellets were resuspended using gentle vortexing in chilled 0.4 N H_2SO_4, followed by a 3 hour incubation while rotating at 4 °C. After centrifugation, supernatants were collected and proteins were precipitated in 20% TCA overnight at 4°C, washed with 0.1% HCl (v/v) acetone once, followed by two washes with acetone alone. Histones were resuspended in deionized water. Acid-extracted histones (20 μg) were resuspended in 50 mM ammonium bicarbonate (pH 8.0), derivatized using propionic anhydride and digested with trypsin as previously described [52–54]. In brief, the lysine residues from histones were derivatized with the propionylation reagent (1:2 reagent:sample ratio) containing acetonitrile and propionic anhydride (3:1), and the solution pH was adjusted to 8.0 using ammonium hydroxide. The propionylation was performed twice and the samples were dried on speed vac. The derivatized histones were then digested with trypsin at a 1:50 ratio (wt/wt) in 50 mM ammonium bicarbonate buffer at 37°C overnight. The N-termini of histone peptides were derivatized with the propionylation reagent twice and dried on speed vac. The peptides were desalted with the self-packed C18 stage tip. The purified peptides were then dried and reconstituted in 0.1% formic acid. Nanoflow liquid chromatography was performed using a Thermo Fisher Scientific, Vanquish Neo UHPLC equipped with an Easy-Spray™ PepMap™ Neo nano-column (2 μm, C18, 75 μm × 150 mm). Buffer A was 0.1% formic acid and Buffer B was 0.1% formic acid in 80% acetonitrile. Peptides were resolved using at room temperature with a mobile phase consisting of a linear gradient from 1 to 45% solvent B (0.1% formic acid in 100% acetonitrile) in solvent A (0.1% formic acid in water) over 85 mins and then 45 to 98% solvent B over 5 mins at a flow rate of 300 nL/min. The HPLC was coupled online to an Orbitrap Exploris 240 (Thermo Scientific) mass spectrometer operating in the positive mode using a Nanospray Flex Ion Source (Thermo Fisher Scientific) at 1.9 kV. To perform the global histone PTM analysis, the mass spectrometer was programmed for data-independent acquisition (DIA). One acquisition cycle consisted of a full MS scan, 35 DIA MS/MS scans of 24 m/z isolation width starting from 290 m/z to reach 1115 m/z. Typically, full MS scans were acquired in the Orbitrap mass analyzer across 290–1115 m/z at a resolution of 60,000 in positive profile mode with a maximum injection time of 60 ms and an AGC target of 300%. MS/MS data from HCD fragmentation was collected in the ion trap (when available) or the Orbitrap. These scans typically used an NCE of 30, an AGC target of 1000%, and a maximum injection time of 60 ms.

RNAseq—RNA was isolated using RNeasy Plus Kit (Qiagen) according to manufacturer's instructions and the quality was assessed with the Agilent 2100 Bioanalyzer with an RNA 6000 Pico Kit (Agilent Technologies). PolyA-enriched RNA libraries were prepared with

the KAPA Stranded mRNA Sample Preparation Kit (Kapa Biosystems). Sequencing was performed with NovaSeq 6000 (Illumina) at a depth of 18–50 million paired reads per sample.

Chromatin immunoprecipitation sequencing (ChIPseq)—ChIP method was adapted from Cook et al., with some modifications [55]. DIPGXIII or SF7761 cells were treated with DMSO or SB939 for 16 hours and collected for fixation with 1% formaldehyde and neutralisation with 0.125 M glycine. Cell pellets were washed twice with ice-cold PBS supplemented with protease inhibitor cocktail. 1.5×10^6 cells were used per each IP. Cells were resuspended in 15 ml of ice-cold buffer A (0.32 M sucrose, 15 mM HEPES, pH 7.9, 60 mM KCl, 2 mM EDTA, 0.5 mM EGTA, 0.5% (w/v) BSA, 0.5 mM DTT, protease inhibitors cocktail) and incubated for 20 min on ice. Subsequently, nuclei were released by passing cell suspension through the Dounce homogenizer (20 strokes) and layering it over 15 ml of buffer A+ (1.3 M sucrose, 15 mM HEPES, pH 7.9, 60 mM KCl, 2 mM EDTA, 0.5 mM EGTA, 0.5% (w/v) BSA, 0.5 mM DTT, protease inhibitors cocktail) in 50 ml falcon tube. After 5 min of centrifugation at 1000 × g and 4 °C, nuclear pellets were washed twice with 10 ml of buffer W (10 mM Tris·Cl, pH 7.4, 15 mM NaCl, 60 mM KCl, protease inhibitors cocktail) and pelleted by 350 × g centrifugation for 4 min at 4 °C. Nuclei were resuspended with 400 µl of buffer W and supplemented with final 1.2 mM $CaCl_2$. Subsequently, 100 µl of nuclease-free water containing 20 units of micrococcal nuclease (MNase, Worthington) was added and enzymatic chromatin digestion was carried out for 25 min at 25°C with 1000 rpm shaking. Reaction was then stopped with 30 µl of 0.5M EDTA and EGTA solutions. Subsequently, chromatin was solubilised with supplementation of 0.5% SDS followed by 10-fold dilution in LB3 buffer (1 mM EDTA, 10 mM Tris·Cl, pH 7.5, 1% (w/v) sodium deoxycholate, 0.5% (w/v) sarkosyl, 1% (v/v) Triton X-100). After 10 min incubation on ice, samples were centrifuged for 10 min at 16000 × g 4 °C and supernatant collected. 200 µl of lysate was taken for input sample and the rest used in over-night immunoprecipitation with 4 µg of antibody and end-over-end rotation at 4 °C. The following antibodies were used for each IP reaction: H3.3 (09–838, Millipore), H3.3K27M (61803, Active Motif) and H2A.Z (ab150402, Abcam). The next day 20 µl of pre-washed Protein A Dynabeads (Invitrogen) were added, and incubation continued for another 2 hours at 4 °C. Beads were then washed 6 times with LB3 buffer and collected using the magnetic stand. Immunoprecipitated chromatin was eluted twice with 125 µl of elution buffer (0.2% (w/v) SDS, 0.1 M $NaHCO_3$, 5 mM DTT) at 65 °C for 10 min. Next, chromatin eluates and inputs were subjected first to reverse crosslinking over night at 65 °C, then to 30 min of RNAse A treatment at 37°C followed by Proteinase K treatment for 4 hours at 50 °C. DNA was then extracted with phenol/chloroform/isoamyl alcohol reagent as previously described and precipitated from the aqueous phase with 3 volumes of 100% ethanol in the presence of 0.1 volume of 3M sodium acetate and 1 ul of glycogen [56]. DNA was additionally purified with ZymoResearch DNA Clean & Concentrator-5 columns (D4003T) and digested DNA profiles confirmed using the 2100 Bioanalyzer with the Agilent DNA High Sensitivity chip (Agilent Technologies). The libraries were then prepared using the Qiaseq Ultra Low Input Library Kit (Qiagen), according to manufacturer's instructions. Sequencing was performed with NovaSeq 6000 or HiSeq1500 (Illumina) at a depth of 20 to 56 million single-end reads.

Quantification and statistical analysis

Statistical analysis of biochemical data—Statistical analyses for qPCRs, immunofluorescent intensity, MTT, BrdU and western blotting quantitation were performed with Student's t-test and/or ANOVA using GraphPad Prism software (GraphPad Software Inc.), as indicated in figure legends. Mean and standard deviations were plotted for three biological replicates, as indicated in individual figure legends. Statistically significant P-value was considered below 0.05 and was denoted with an actual number for each analysis (ns, non-significant p value).

RNAseq analysis—The sequenced paired-end reads were mapped to hg38 genome using tophat2 aligner v2.1.1 with the default parameters. The expression estimates for each gene were obtained using Bioconductor package DESeq2. TPM (Transcripts per Kilobase Million) values were calculated and used to perform all visualizations and all analyses besides differential expression. Genes that had significant (Benjamini and Hochberg-corrected P <0.05 and |log2(Fold Change)|>1) changes in their expression levels were called as differentially expressed. All gene ontology analyses were performed with GO.db Bioconductor package and 0.05 significance threshold on Bonferroni corrected P-value (Fisher's exact test). All statistical analyses were performed in R programming environment (http://r-project.org). The H3.3K27M signature was obtained from Bender et al. [12]. External data sets were downloaded from the GEO database for cells treated with panobinostat. We used expression profiles for BT245 and DIPGXIII from GSE117446 [31], and DIPGIV and DIPGXIII from GSE94259 [26]. The used H3.3K27M KO and wild-type gene expression profiles stored under GSE117446 [31]. The RNAseq data generated in this project were deposited at the NCBI platform under GSE232283 Number.

ChIPseq analysis—The paired-end fragments were generated. Reads were mapped to the to hg38 genome using Bowtie aligner version 0.12.9. Only uniquely mapped reads were retained. The reads with insert sizes <50 bp or >500 bp were removed from further analysis. Genomic positions with the numbers of mapped tags above the significance threshold of Z-score of 7 were identified as anomalous, and the tags mapped to such positions were discarded [57]. H2A.Z, H3.3 and H3.3K27M occupancies were estimated as tag frequencies. Input correction was not used in line with previous study [58]. Enrichment peaks were called with MACS2.0 (q-value< 0.0001 and log2(Fold Change > 2)). The ChIPseq data generated in this project was deposited at NCBI under GSE232283 Number. The used publicly available H3.3K27M ChIP-seq results were obtained from GSE163184 and GSE78801 [59,60].

MS data analysis—Raw files were analyzed using EpiProfile 2.0 [61]. The area for each modification state of a peptide was normalized against the total signal for that peptide to give the relative abundance of the histone modification. To identify the H3.3K27M peptides, a full MS scan was acquired in the Orbitrap mass analyzer across 350–1050 m/z at a resolution of 120,000 in positive profile mode with an auto maximum injection time and an AGC target of 300%. Parallel reaction monitoring experiments were followed for monitoring the targeted peptides based on the inclusion list (Supplementary Table S4). Targeted ions were fragmented using HCD fragmentation. These scans typically used an

NCE of 30, an AGC target standard, and an auto maximum injection time. The targeted peptides were analysed on Skyline [62]. The data was deposited at the MassIVE database under the accession number MSV000093052. The peptide PRM target list is included in the Supplementary Table 1.

Supplementary Material

Refer to Web version on PubMed Central for supplementary material.

ACKNOWLEDGEMENTS

We thank Prof. Ester Hammond (University of Oxford) for the critical reading of the manuscript. We acknowledge Sequencing Lab at the Nencki Institute for performing all NGS sequencings.

FUNDING

This work was supported by the National Science Center, Poland grant (award no. 2017/27/B/NZ2/02827) to JM (Mieczkowski). Part of JM (Mieczkowski)'s and KBL's salaries were founded by Foundation for Polish Science (FNP) under the International Research Agendas Program (grant number MAB/2018/6) and the National Science Center, Poland grant (award no. 2019/33/B/NZ1/01556), respectively. BAG was supported by NIH grants P01CA196539 and R01HD106051. JM (Majewski) was supported by NIH P01CA196539 and CIHR PJT-183939 grants.

REFERENCES

1. Kornberg RD (1974). Chromatin structure: A repeating unit of histones and DNA. Science (80-.). 184, 868–871.
2. Buschbeck M, and Hake SB (2017). Variants of core histones and their roles in cell fate decisions, development and cancer. Nat. Rev. Mol. Cell Biol 18, 299–314. [PubMed: 28144029]
3. Maze I, Noh KM, Soshnev AA, and Allis CD (2014). Every amino acid matters: Essential contributions of histone variants to mammalian development and disease. Nat. Rev. Genet 15, 259–71. [PubMed: 24614311]
4. O'Donnell A, Yang SH, and Sharrocks AD (2013). PARP1 orchestrates variant histone exchange in signal-mediated transcriptional activation. EMBO Rep. 14, 1084–1091. [PubMed: 24145797]
5. Coleman-Derr D, and Zilberman D (2012). Deposition of Histone Variant H2A.Z within Gene Bodies Regulates Responsive Genes. PLoS Genet. 8, e1002988. [PubMed: 23071449]
6. Subramanian V, Fields PA, and Boyer LA (2015). H2A.Z: A molecular rheostat for transcriptional control. F1000Prime Rep. 7, 1–10.
7. Ahmad K, and Henikoff S (2002). The histone variant H3.3 marks active chromatin by replication-independent nucleosome assembly. Mol. Cell 9, 1191–200. [PubMed: 12086617]
8. Goldberg AD, Banaszynski LA, Noh KM, Lewis PW, Elsaesser SJ, Stadler S, Dewell S, Law M, Guo X, Li X, et al. (2010). Distinct Factors Control Histone Variant H3.3 Localization at Specific Genomic Regions. Cell 140, 678–91. [PubMed: 20211137]
9. Bonner ER, Dawood A, Gordish-Dressman H, Eze A, Bhattacharya S, Yadavilli S, Mueller S, Waszak SM, and Nazarian J (2023). Pan-cancer atlas of somatic core and linker histone mutations. NPJ Genomic Med. 8, 1–14.
10. Chan KM, Fang D, Gan H, Hashizume R, Yu C, Schroeder M, Gupta N, Mueller S, David James C, Jenkins R, et al. (2013). The histone H3.3K27M mutation in pediatric glioma reprograms H3K27 methylation and gene expression. Genes Dev. 27, 985–990. [PubMed: 23603901]
11. Lewis PW, Müller MM, Koletsky MS, Cordero F, Lin S, Banaszynski LA, Garcia BA, Muir TW, Becher OJ, and Allis CD (2013). Inhibition of PRC2 activity by a gain-of-function H3 mutation found in pediatric glioblastoma. Science (80-.). 340, 857–61.
12. Bender S, Tang Y, Lindroth AM, Hovestadt V, Jones DTW, Kool M, Zapatka M, Northcott PA, Sturm D, Wang W, et al. (2013). Reduced H3K27me3 and DNA Hypomethylation Are Major

Drivers of Gene Expression in K27M Mutant Pediatric High-Grade Gliomas. Cancer Cell 24, 660–672. [PubMed: 24183680]

13. Schwartzentruber J, Korshunov A, Liu XY, Jones DTW, Pfaff E, Jacob K, Sturm D, Fontebasso AM, Quang DAK, Tönjes M, et al. (2012). Driver mutations in histone H3.3 and chromatin remodelling genes in paediatric glioblastoma. Nature 482, 226–31. [PubMed: 22286061]
14. Castel D, Kergrohen T, Tauziède-Espariat A, Mackay A, Ghermaoui S, Lechapt E, Pfister SM, Kramm CM, Boddaert N, Blauwblomme T, et al. (2020). Histone H3 wild-type DIPG/DMG overexpressing EZHIP extend the spectrum diffuse midline gliomas with PRC2 inhibition beyond H3-K27M mutation. Acta Neuropathol. 139, 1109–1113. [PubMed: 32193787]
15. Diehl KL, Ge EJ, Weinberg DN, Jani KS, Allis CD, and Muir TW (2019). PRC2 engages a bivalent H3K27M-H3K27me3 dinucleosome inhibitor. Proc. Natl. Acad. Sci. U. S. A 116, 22152–22157. [PubMed: 31611394]
16. Fang D, Gan H, Cheng L, Lee JH, Zhou H, Sarkaria JN, Daniels DJ, and Zhang Z (2018). H3.3K27M mutant proteins reprogram epigenome by sequestering the PRC2 complex to poised enhancers. Elife 7, e36696. [PubMed: 29932419]
17. Justin N, Zhang Y, Tarricone C, Martin SR, Chen S, Underwood E, De Marco V, Haire LF, Walker PA, Reinberg D, et al. (2016). Structural basis of oncogenic histone H3K27M inhibition of human polycomb repressive complex 2. Nat. Commun 7, 11316. [PubMed: 27121947]
18. Chen KY, Bush K, Klein RH, Cervantes V, Lewis N, Naqvi A, Carcaboso AM, Lechpammer M, and Knoepfler PS (2020). Reciprocal H3.3 gene editing identifies K27M and G34R mechanisms in pediatric glioma including NOTCH signaling. Commun. Biol 3, 363. [PubMed: 32647372]
19. Filbin MG, Tirosh I, Hovestadt V, Shaw ML, Escalante LE, Mathewson ND, Neftel C, Frank N, Pelton K, Hebert CM, et al. (2018). Developmental and oncogenic programs in H3K27M gliomas dissected by single-cell RNA-seq. Science (80-.). 360, 331–335.
20. Harutyunyan AS, Krug B, Chen H, Papillon-Cavanagh S, Zeinieh M, De Jay N, Deshmukh S, Chen CCL, Belle J, Mikael LG, et al. (2019). H3K27M induces defective chromatin spread of PRC2-mediated repressive H3K27me2/me3 and is essential for glioma tumorigenesis. Nat. Commun 10, 1262. [PubMed: 30890717]
21. Silveira AB, Kasper LH, Fan Y, Jin H, Wu G, Shaw TI, Zhu X, Larson JD, Easton J, Shao Y, et al. (2019). H3.3 K27M depletion increases differentiation and extends latency of diffuse intrinsic pontine glioma growth in vivo. Acta Neuropathol. 137, 637–655. [PubMed: 30770999]
22. Leszczynska KB, Jayaprakash C, Kaminska B, and Mieczkowski J (2021). Emerging Advances in Combinatorial Treatments of Epigenetically Altered Pediatric High-Grade H3K27M Gliomas. Front. Genet 12, 742561. [PubMed: 34646308]
23. Grasso CS, Tang Y, Truffaux N, Berlow NE, Liu L, Debily MA, Quist MJ, Davis LE, Huang EC, Woo PJ, et al. (2015). Functionally defined therapeutic targets in diffuse intrinsic pontine glioma. Nat. Med 21, 555–559. [PubMed: 25939062]
24. Anastas JN, Zee BM, Kalin JH, Kim M, Guo R, Alexandrescu S, Blanco MA, Giera S, Gillespie SM, Das J, et al. (2019). Re-programing Chromatin with a Bifunctional LSD1/HDAC Inhibitor Induces Therapeutic Differentiation in DIPG. Cancer Cell 36, 528–544.e10. [PubMed: 31631026]
25. Brown ZZ, Müller MM, Jain SU, Allis CD, Lewis PW, and Muir TW (2014). Strategy for "Detoxification" of a cancer-derived histone mutant based on mapping its interaction with the methyltransferase PRC2. J. Am. Chem. Soc 136, 13498–13501. [PubMed: 25180930]
26. Nagaraja S, Vitanza NA, Woo PJ, Taylor KR, Liu F, Zhang L, Li M, Meng W, Ponnuswami A, Sun W, et al. (2017). Transcriptional Dependencies in Diffuse Intrinsic Pontine Glioma. Cancer Cell 31, 635–652.e6. [PubMed: 28434841]
27. Lin GL, Wilson KM, Ceribelli M, Stanton BZ, Woo PJ, Kreimer S, Qin EY, Zhang X, Lennon J, Nagaraja S, et al. (2019). Therapeutic strategies for diffuse midline glioma from high-throughput combination drug screening. Sci. Transl. Med 11, eaaw0064. [PubMed: 31748226]
28. Mackay A, Burford A, Carvalho D, Izquierdo E, Fazal-Salom J, Taylor KR, Bjerke L, Clarke M, Vinci M, Nandhabalan M, et al. (2017). Integrated Molecular Meta-Analysis of 1,000 Pediatric High-Grade and Diffuse Intrinsic Pontine Glioma. Cancer Cell 32, 520–537.e5. [PubMed: 28966033]

29. Hashizume R, Andor N, Ihara Y, Lerner R, Gan H, Chen X, Fang D, Huang X, Tom MW, Ngo V, et al. (2014). Pharmacologic inhibition of histone demethylation as a therapy for pediatric brainstem glioma. Nat. Med 20, 1394–1396. [PubMed: 25401693]
30. Harutyunyan AS, Chen H, Lu T, Horth C, Nikbakht H, Krug B, Russo C, Bareke E, Marchione DM, Coradin M, et al. (2020). H3K27M in Gliomas Causes a One-Step Decrease in H3K27 Methylation and Reduced Spreading within the Constraints of H3K36 Methylation. Cell Rep. 33, 108390. [PubMed: 33207202]
31. Krug B, De Jay N, Harutyunyan AS, Deshmukh S, Marchione DM, Guilhamon P, Bertrand KC, Mikael LG, McConechy MK, Chen CCL, et al. (2019). Pervasive H3K27 Acetylation Leads to ERV Expression and a Therapeutic Vulnerability in H3K27M Gliomas. Cancer Cell 35, 782–797.e8. [PubMed: 31085178]
32. Venkatesh HS, Tam LT, Woo PJ, Lennon J, Nagaraja S, Gillespie SM, Ni J, Duveau DY, Morris PJ, Zhao JJ, et al. (2017). Targeting neuronal activity-regulated neuroligin-3 dependency in high-grade glioma. Nature 549.
33. Venkatesh HS, Johung TB, Caretti V, Noll A, Tang Y, Nagaraja S, Gibson EM, Mount CW, Polepalli J, Mitra SS, et al. (2015). Neuronal activity promotes glioma growth through neuroligin-3 secretion. Cell 161, 803–16. [PubMed: 25913192]
34. Lan YY, Londoño D, Bouley R, Rooney MS, and Hacohen N (2014). Dnase2a deficiency uncovers lysosomal clearance of damaged nuclear DNA via autophagy. Cell Rep. 9, 180–192. [PubMed: 25284779]
35. Hormazabal J, Saavedra F, Espinoza-Arratia C, Martinez NW, Cruces T, Alfaro IE, and Loyola A (2022). Chaperone mediated autophagy contributes to the newly synthesized histones H3 and H4 quality control. Nucleic Acids Res. 50, 1875–1887. [PubMed: 35037039]
36. Valdés-Mora F, Song JZ, Statham AL, Strbenac D, Robinson MD, Nair SS, Patterson KI, Tremethick DJ, Stirzaker C, and Clark SJ (2012). Acetylation of H2A.Z is a key epigenetic modification associated with gene deregulation and epigenetic remodeling in cancer. Genome Res. 22, 307–321. [PubMed: 21788347]
37. Jin C, and Felsenfeld G (2007). Nucleosome stability mediated by histone variants H3.3 and H2A.Z. Genes Dev. 21, 1519–1529. [PubMed: 17575053]
38. Chen P, Zhao J, Wang Y, Wang M, Long H, Liang D, Huang L, Wen Z, Li W, Li X, et al. (2013). H3.3 actively marks enhancers and primes gene transcription via opening higher-ordered chromatin. Genes Dev. 27, 2109–2124. [PubMed: 24065740]
39. Li G. De (2006). Nucleus may be the key site of chloroquine antimalarial action and resistance development. Med. Hypotheses 67, 323–6. [PubMed: 16549276]
40. Hoelper D, Huang H, Jain AY, Patel DJ, and Lewis PW (2017). Structural and mechanistic insights into ATRX-dependent and -independent functions of the histone chaperone DAXX. Nat. Commun 8, 1193. [PubMed: 29084956]
41. Henikoff S (2009). Labile H3.3+H2A.Z nucleosomes mark “nucleosome-free regions.” Nat. Genet 41, 865–6. [PubMed: 19639024]
42. Ávila-López PA, Nuñez-Martínez HN, Peralta-Alvarez CA, Martinez-Calvillo S, Recillas-Targa F, and Hernández-Rivas R (2022). Interplay Between the Histone Variant H2A.Z and the Epigenome in Pancreatic Cancer. Arch. Med. Res 53, 840–858. [PubMed: 36470770]
43. Ávila-López PA, Guerrero G, Nuñez-Martínez HN, Peralta-Alvarez CA, Hernández-Montes G, Álvarez-Hilario LG, Herrera-Goepfert R, Albores-Saavedra J, Villegas-Sepúlveda N, Cedillo-Barrón L, et al. (2021). H2A.Z overexpression suppresses senescence and chemosensitivity in pancreatic ductal adenocarcinoma. Oncogene 40, 2065–2080. [PubMed: 33627784]
44. Huang C, Zhang Z, Xu M, Li Y, Li Z, Ma Y, Cai T, and Zhu B (2013). H3.3-H4 Tetramer Splitting Events Feature Cell-Type Specific Enhancers. PLoS Genet. 9, e1003558. [PubMed: 23754967]
45. Mueller S, Hashizume R, Yang X, Kolkowitz I, Olow AK, Phillips J, Smirnov I, Tom MW, Prados MD, James CD, et al. (2014). Targeting wee1 for the treatment of pediatric high-grade gliomas. Neuro. Oncol 16, 352–60. [PubMed: 24305702]
46. Hashizume R, Smirnov I, Liu S, Phillips JJ, Hyer J, McKnight TR, Wendland M, Prados M, Banerjee A, Nicolaides T, et al. (2012). Characterization of a diffuse intrinsic pontine glioma cell

line: Implications for future investigations and treatment. J. Neurooncol 110, 305–313. [PubMed: 22983601]

47. Kline C, Jain P, Kilburn L, Bonner ER, Gupta N, Crawford JR, Banerjee A, Packer RJ, Villanueva-Meyer J, Luks T, et al. (2022). Upfront Biology-Guided Therapy in Diffuse Intrinsic Pontine Glioma: Therapeutic, Molecular, and Biomarker Outcomes from PNOC003. Clin. Cancer Res 28, 3965–3978. [PubMed: 35852795]
48. Mueller T, Laternser S, Guerreiro Stücklin AS, Gerber NU, Mourabit S, Rizo M, Rushing EJ, Kottke R, Grotzer M, Krayenbühl N, et al. (2023). Real-time drug testing of paediatric diffuse midline glioma to support clinical decision making: The Zurich DIPG/DMG centre experience. Eur. J. Cancer 178, 171–179. [PubMed: 36455411]
49. Przystal JM, Cosentino CC, Yadavilli S, Zhang J, Laternser S, Bonner ER, Prasad R, Dawood AA, Lobeto N, Chong WC, et al. (2022). Imipridones affect tumor bioenergetics and promote cell lineage differentiation in diffuse midline gliomas. Neuro. Oncol 24, 1438–1451. [PubMed: 35157764]
50. Przystal JM, Park I, Zhang J, Hadaczek P, Bankiewicz K, Gupta N, Nazarian J, and Mueller S (2023). Efficacy of convection enhanced delivery of MTX110 (soluble panobinostat) in preclinical Diffuse Intrinsic Pontine Glioma models using metabolic hyperpolarized 13C imaging. EJC Paediatr. Oncol 2, 100021.
51. Ciechomska IA, Wojnicki K, Wojtas B, Szadkowska P, Poleszak K, Kaza B, Jaskula K, Dawidczyk W, Czepko R, Banach M, et al. (2023). Exploring Novel Therapeutic Opportunities for Glioblastoma Using Patient-Derived Cell Cultures. Cancers (Basel). 15, 1562. [PubMed: 36900355]
52. Farhangdoost N, Horth C, Hu B, Bareke E, Chen X, Li Y, Coradin M, Garcia BA, Lu C, and Majewski J (2021). Chromatin dysregulation associated with NSD1 mutation in head and neck squamous cell carcinoma. Cell Rep. 34, 108769. [PubMed: 33626351]
53. Sidoli S, Bhanu NV, Karch KR, Wang X, and Garcia BA (2016). Complete workflow for analysis of histone post-translational modifications using bottom-up mass spectrometry: From histone extraction to data analysis. J. Vis. Exp 2016, 54112.
54. Bhanu NV, Sidoli S, and Garcia BA (2020). A Workflow for Ultra-rapid Analysis of Histone Post-translational Modifications with Direct-injection Mass Spectrometry. Bio-protocol 10, e3756. [PubMed: 33659415]
55. Cook A, Mieczkowski J, and Tolstorukov MY (2017). Single-assay profiling of nucleosome occupancy and chromatin accessibility. Curr. Protoc. Mol. Biol 2017, 21.34.1–21.34.18.
56. Moore D, and Dowhan D (2002). Purification and concentration of DNA from aqueous solutions. Curr. Protoc. Mol. Biol Chapter 2, Unit 2.1A.
57. Tolstorukov MY, Goldman JA, Gilbert C, Ogryzko V, Kingston RE, and Park PJ (2012). Histone Variant H2A.Bbd Is Associated with Active Transcription and mRNA Processing in Human Cells. Mol. Cell 47, 596–607. [PubMed: 22795134]
58. Mueller B, Mieczkowski J, Kundu S, Wang P, Sadreyev R, Tolstorukov MY, and Kingston RE (2017). Widespread changes in nucleosome accessibility without changes in nucleosome occupancy during a rapid transcriptional induction. Genes Dev. 31, 451–462. [PubMed: 28356342]
59. Piunti A, Hashizume R, Morgan MA, Bartom ET, Horbinski CM, Marshall SA, Rendleman EJ, Ma Q, Takahashi YH, Woodfin AR, et al. (2017). Therapeutic targeting of polycomb and BET bromodomain proteins in diffuse intrinsic pontine gliomas. Nat. Med 23, 493–500. [PubMed: 28263307]
60. Furth N, Algranati D, Dassa B, Beresh O, Fedyuk V, Morris N, Kasper LH, Jones D, Monje M, Baker SJ, et al. (2022). H3-K27M-mutant nucleosomes interact with MLL1 to shape the glioma epigenetic landscape. Cell Rep. 39, 110836. [PubMed: 35584667]
61. Yuan ZF, Lin S, Molden RC, Cao XJ, Bhanu NV, Wang X, Sidoli S, Liu S, and Garcia BA (2015). Epiprofile quantifies histone peptides with modifications by extracting retention time and intensity in high-resolution mass spectra. Mol. Cell. Proteomics 14, 1696–707. [PubMed: 25805797]
62. MacLean B, Tomazela DM, Shulman N, Chambers M, Finney GL, Frewen B, Kern R, Tabb DL, Liebler DC, and MacCoss MJ (2010). Skyline: An open source document editor for creating and analyzing targeted proteomics experiments. Bioinformatics 26, 966–8. [PubMed: 20147306]

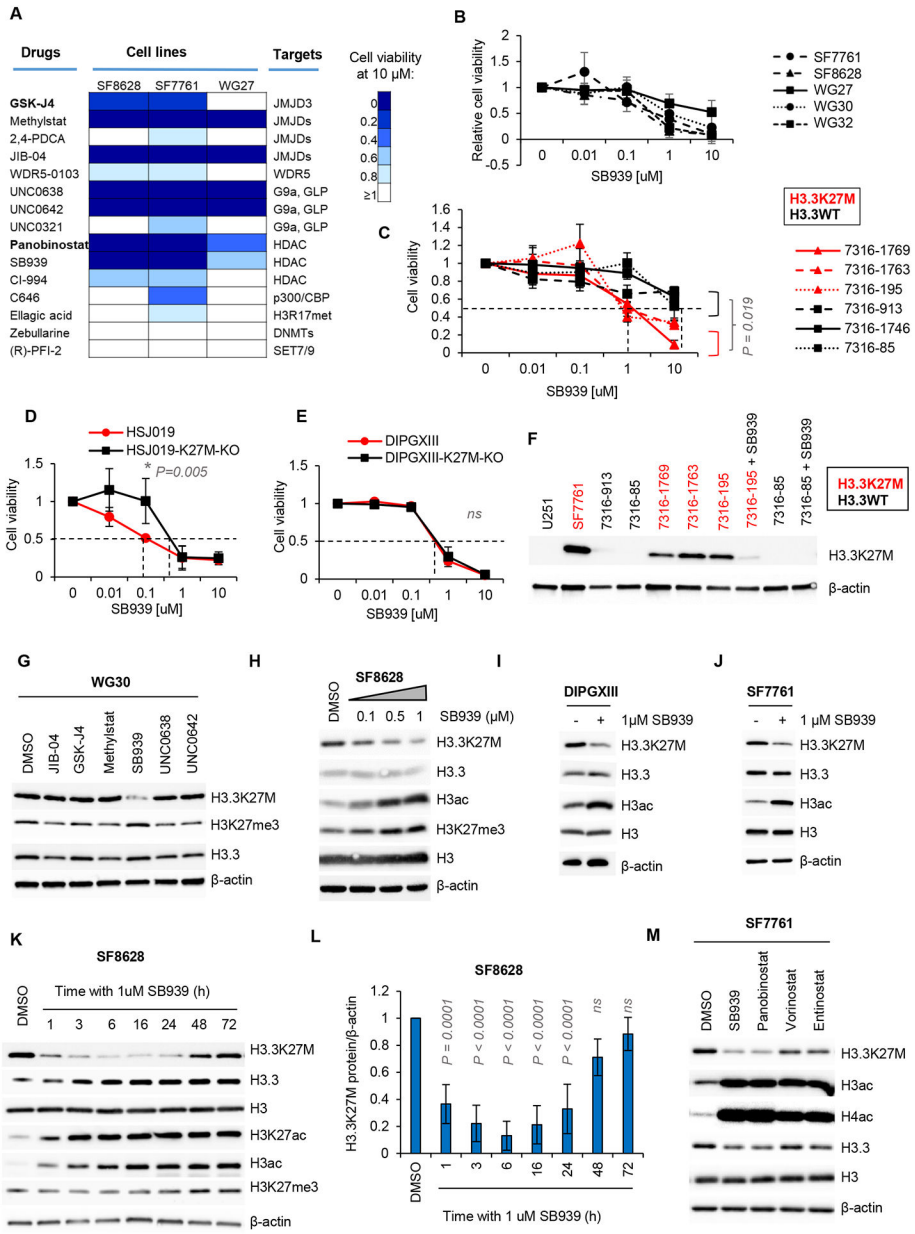

Figure 1. Epigenetic inhibitor screening in H3K27M-expressing paediatric high-grade glioma cells revealed HDACi-dependent decrease of the H3.3K27M oncohistone

A. SF8628, SF7761 and WG27 cells were treated for 72 hours with the indicated drugs (10 μM) and subjected to cell viability assay (MTT metabolism). Darker blue colours (legend closer to 0) show stronger cell killing by a particular drug. GSK-J4 and Panobinostat are shown as positive controls.

B. SF7761, SF8628, WG27, WG30, WG32 cell lines expressing H3.3K27M were treated with serial dilutions of SB939, as indicated, and their cell viability was assessed after 72 hours by MTT assay. Mean cell viability and standard deviation (SD) is plotted from three independent experiments.

C. Patient-derived pHGG neurospheres expressing either H3.3K27M (red) or wild-type (WT) H3.3 (black) were treated with SB939 at increasing cell concentrations. Cell viability

was assessed; mean cell viability and s.d. is plotted from three independent experiments. Two-way ANOVA test showed statistically significant difference between the H3.3K27M and H3.3 WT groups of cells (P=0.019). Multiple comparison showed significant differences at 1 and 10 μM treatments (adjusted P value of 0.002 and 0.003, respectively).

D–E. HSJ019 and DIPGXIII pHGG-derived cells expressing H3.3K27M and their isogenic pairs with the deleted *H3F3A* mutated allele (K27M-KO) were treated with SB939 at dilutions shown and assessed for cell viability. Data is shown as mean cell viability and s.d. from three independent experiments. Two-way ANOVA test between parental ($H3.3K27M^{+}$) and K27M-KO cells shows statistically significant difference only for HSJ019 cell line in **D** (adjusted P = 0.005).

F. Presence of the histone H3.3 mutation resulting in pH3.3K27M substitution was verified by Western blotting of cell lysates. 24-hour treatment with 1 μM SB939 was included as indicated.

G. SB939-dependent decrease in H3.3K27M protein levels in WG30 cells treated with selected drugs from **A** as demonstrated by Western blotting.

H. A dose-dependent decrease of H3.3K27M protein after 48 hours of SB939 treatment shown by Western blotting. A representative experiment of three independent repeats is shown.

I–J. The H3.3K27M protein levels 16 hours of SB939 treatment in DIPGXIII (**I**) and SF7761 (**J**) cells as shown by Western blotting. A representative experiment of three independent repeats is shown.

K. Time-dependent decrease of H3.3K27M levels in response to SB939 treatment as shown by Western blotting. A representative experiment of three independent repeats is shown.

L. Densitometry of H3.3K27M blots relative to β-actin from (**K)** shows mean and s.d. from three independent experiments. Statistically significant changes (P<0.0001) were calculated with one-way ANOVA. Dunnett's multiple comparisons test shows differences for each time-point in relation to DMSO control (adjusted P values indicated on the graph).

M. Histone protein expression levels in SF7761 spheres treated for 24 hours with HDAC inhibitors: SB939 (1 μM), panobinostat (0.05 μM), Vorinostat (1 μM), Entinostat (1 μM) or DMSO control. Total protein extracts were analysed by Western blotting with the antibodies indicated. A representative blot for 3 independent experiments is shown.

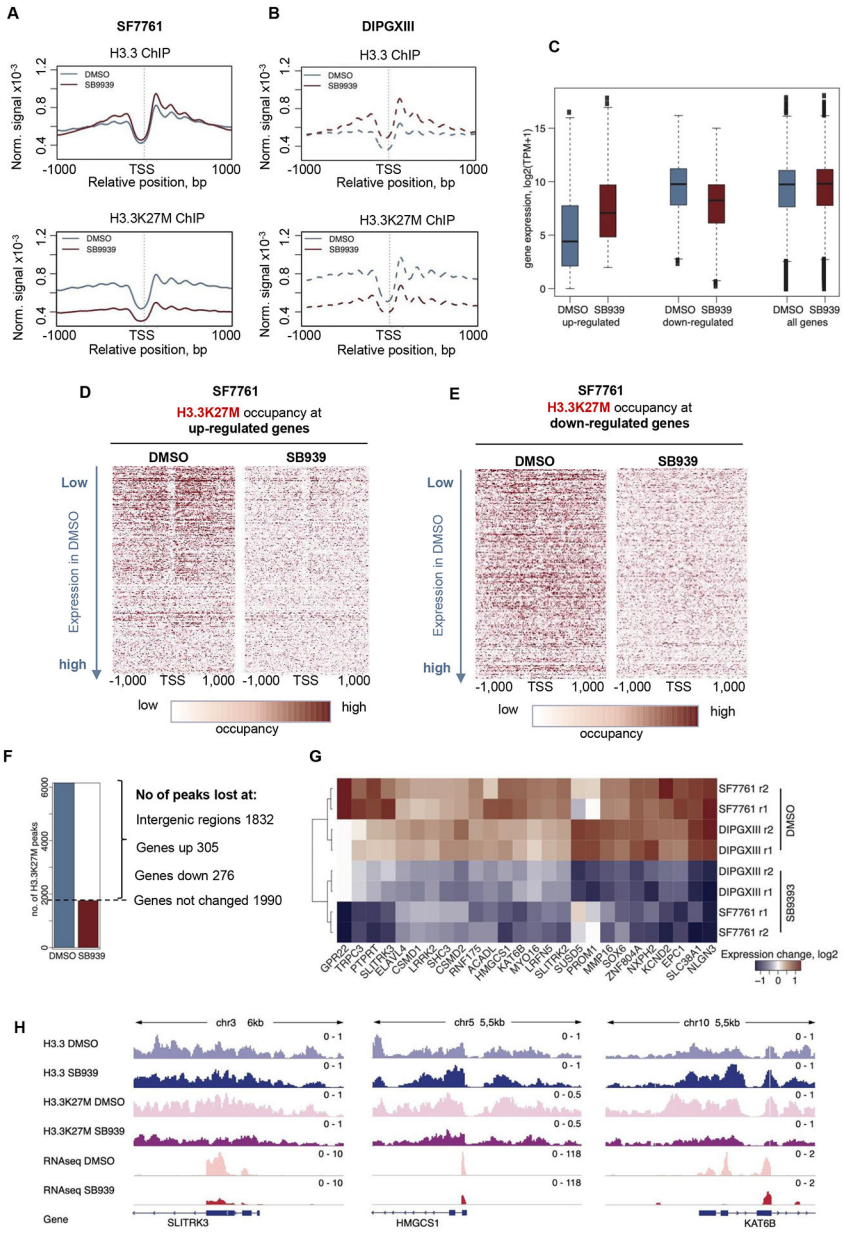

Figure 2. SB939 treatment leads to the loss of H3.3K27M occupancy at the chromatin and specific transcriptomic changes.

A-B. ChIP-seq results for H3.3 (top panel) and H3.3K37M (bottom panel) profiles around TSS (+/−1 kb) of all protein-coding genes in the SF7761 (**A**) and DIPGXIII (**B**) cells treated with DMSO (blue) or 1 μM SB9393 (red) for 16 hours.

C. Average gene expression levels in the sets of up- or down-regulated genes in SF7761 and DIPGXIII cells at 16 hours after 1 μM SB939 treatment is shown (red). Gene expression in DMSO controls is shown in blue.

D–E. Heatmaps showing the H3.3K27M occupancy at up-regulated (**D**) and down-regulated (**E**) genes in SF7761 cells. For each pair, the left and right heatmaps correspond to cells treated for 16 hours with DMSO or 1 μM SB939, respectively. Rows in all heatmaps were

ordered by the gene expression level in control DMSO-treated cells (the lowest expression in DMSO at the top).

F. The number of identified H3.3K27M peaks. The peaks were identified in both cell lines separately and only numbers of overlapped peaks are reported. The blue and the red bars correspond to cells treated for 16 hours with DMSO or SB939, respectively. The genomic distribution is reported for the peaks lost after the SB939 treatment.

G. Heatmap showing normalised (z-scores) gene expression of 26 genes positively associated with the presence of the H3.3K27M oncohistone based on Bender et al. [12]. Treatment with SB939 shows decreased expression of these genes (blue).

H. Example IGV profiles illustrating H3.3K27M loss in SF7761 cells after SB939 treatment at down-regulated genes are shown. Profiles of H3.3, H3.3K27M ChIP-seq and RNA-seq are shown for DMSO or SB939 treatment. Profiles were scaled for each gene locus individually.

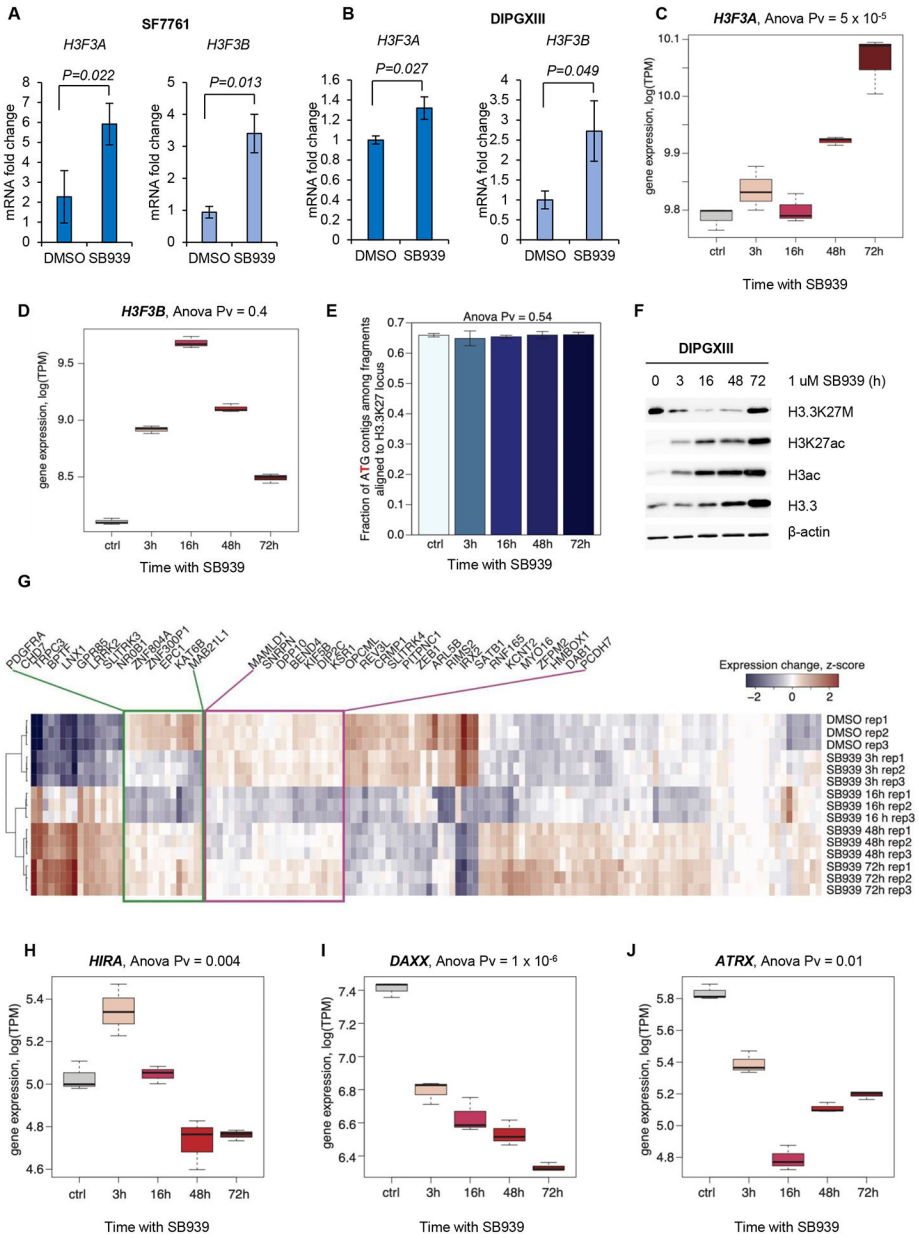

Figure 3. SB939-dependent loss of H3.3K27M is irrespective of *H3F3A* mRNA expression

A–B. Expression of *H3F3A* and *H3F3B* mRNA after 16 hours of treatment with SB939 was tested with qPCR in SF7761 (A) and DIPGXIII (B) cells. *GAPDH* was used as a housekeeping gene. Mean expression and s.d. is shown from three independent experiments. Two-tailed student's t-tests determined the statistical significance, as indicated with *P* values.

C–D. RNAseq of DIPGXIII cells treated with SB939 (1 μM, 3–72 hours) was carried probing for expression of *H3F3A* (**C**) and *H3F3B* (**D**) transcripts.

E. Fraction of RNAseq reads with ATG contig of all sequences aligned to H3.3 lysine 27 locus. Control (ctrl) stands for DMSO, and colours represent time points after SB939 treatment. The analysis was computed for three independent replicates. The fraction was

computed as number of reads with mutated sequences (ATG) to number of total sequences aligned to H3.3 K27 locus. Bars and whiskers correspond to average and standard deviation respectively. P-value shown above the plot was computed with one-way anova test. The analysis was done for DIPGXIII cell line.

F. Western blotting corresponding for the samples from DIPGXIII cells treated as in C-D shows expression of indicated histones and control β-actin.

G. Heatmap showing gene expression changes (z-scores) of 143 genes previously reported as H3K27M-dependent [12] in the SB939 time course treatment analysis from Figure 3C–D. Conditions and replicates are indicated in the right-hand side. The profiles were clustered using hierarchical method.

H–J. Expression of HIRA, DAXX and ATRX histone H3.3 chaperones is plotted for samples from Figure 3C–D.

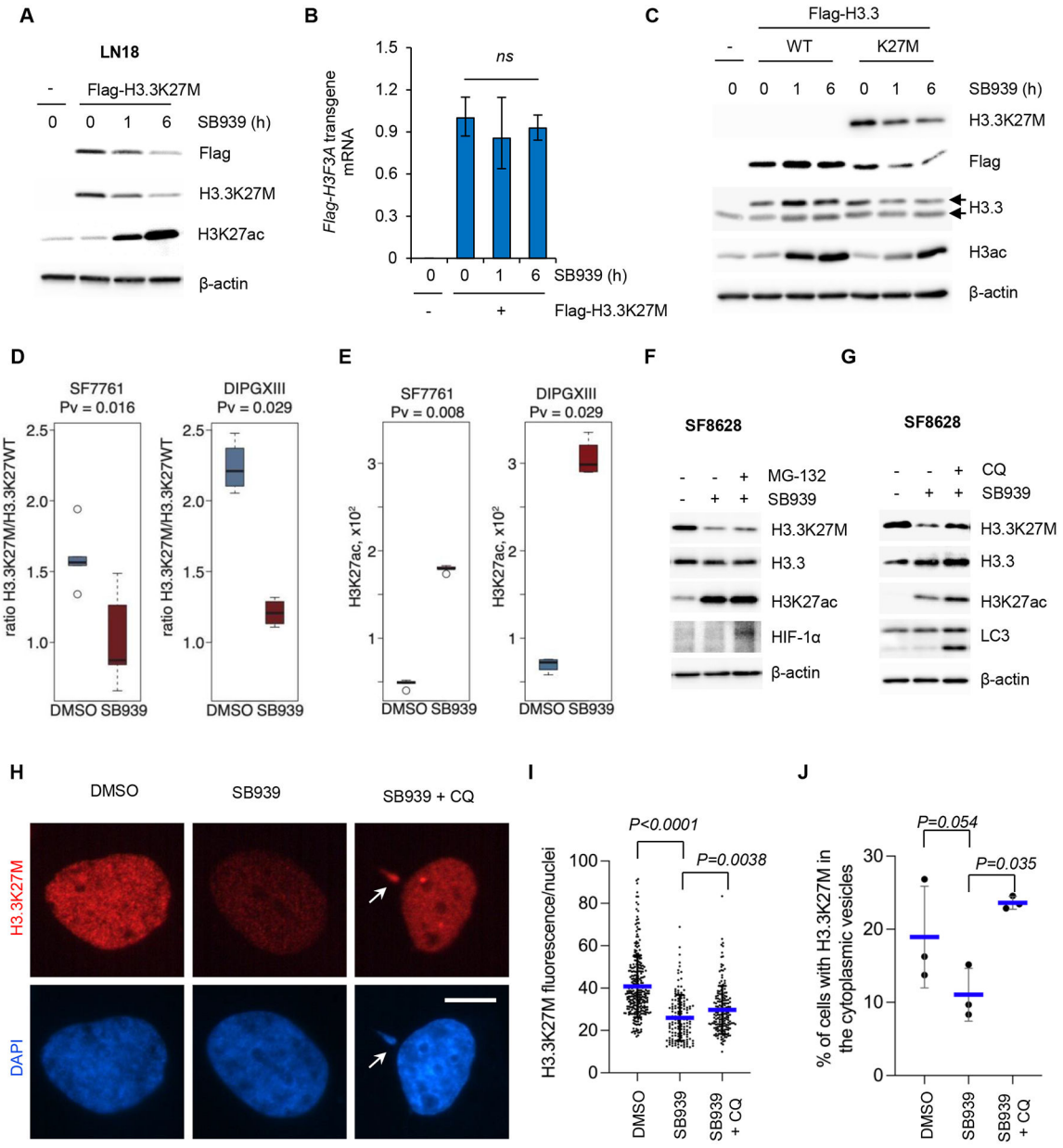

Figure 4. SB939 leads to the specific loss of H3.3K27M protein, which is partially reversed via chloroquine treatment

A. LN18 cells were transfected with Flag-H3.3K27M and 48 hours later exposed to 1 μM SB939 for the times indicated. Western blotting with anti-Flag and anti-H3.3K27M antibodies indicates downregulation of the H3.3K27M protein.

B. Expression of Flag-H3.3K27M transgene in experiment shown in C was confirmed by qPCR with forward primer containing Flag sequence and reverse primer binding within *H3F3A* coding sequence. *GAPDH* was used as a housekeeping gene.

C. LN18 cells were transfected either with Flag-H3.3K27M of Flag-H3.3WT (as indicated) and 48 hours later exposed to 1 μM SB939 for the indicated times. Western blotting with anti-Flag, anti-H3.3K27M And anti-H3.3 antibodies shows expression of transfected histones, accordingly. The top arrow at the H3.3 blot indicates the overexpressed flag-tagged

protein and the lower arrow indicates the endogenous H3.3 protein. A representative experiment from 3 independent repeats is shown.

D. Distribution of ratio of H3.3K27M (H3.3K27M_27–40) versus H3.3 wild type (H3.3K27WT_27–40) peptides analysed with mass spectrometry in SF7761 and DIPGXIII cell-lines treated for 16 hours with DMSO control or with SB939, as indicated.

E. Distribution of H3K27ac_27–40 peptides analysed with mass spectrometry in SF7761 and DIPGXIII cell-lines treated for 16 hours with DMSO control or with SB939, as indicated.

F. SF8628 cells were treated for 1h with 1 μM SB939 in the presence or absence of 1 μM MG-132 proteasome inhibitor. Western blotting was performed with the indicated antibodies. HIF-1α rescue with MG-132 was shown as a positive control for the proteasome inhibition. A representative experiment is shown for three independent repeats.

G. SF8628 cells were treated for 1h with 1 μM SB939 in the presence or absence of 200 μM chloroquine (CQ). Western blotting was performed with the indicated antibodies. LC3 lipidation is shown as a positive control for CQ treatment. A representative experiment is shown for three independent repeats.

H. Cells were seeded on coverslips and 24 hours later were exposed to SB939 and CQ treatment for 1 hour, as indicated. Immunofluorescent staining of H3.3K27M (red) and nuclei (DAPI, blue) was performed, as shown with the representative images. White arrows in the bottom panel indicate example vesicles quantified in **J**. Scale bar, 10 μm.

I. Quantitation of nuclear fluorescence intensity of H3.3K27M staining from **H** was performed for three independent experiments and over 100 of cells were analysed in each condition. Mean intensity per cell (blue line) and standard deviation (black error bars) are overlayed on the top of all measured nuclei in each condition. Unpaired student’s t-test was used to determine statistical significance, as indicated with *P* values.

J. A graph showing % of cells with extranuclear vesicles positive for DNA (DAPI, blue) and H3.3K27M (red) in each treatment condition (example vesicles indicated with white arrows in **H**). A mean % from three independent experiments (blue line) and standard deviation are shown. Paired student’s t-test was used to determine statistical significance, as indicated with *P* values.

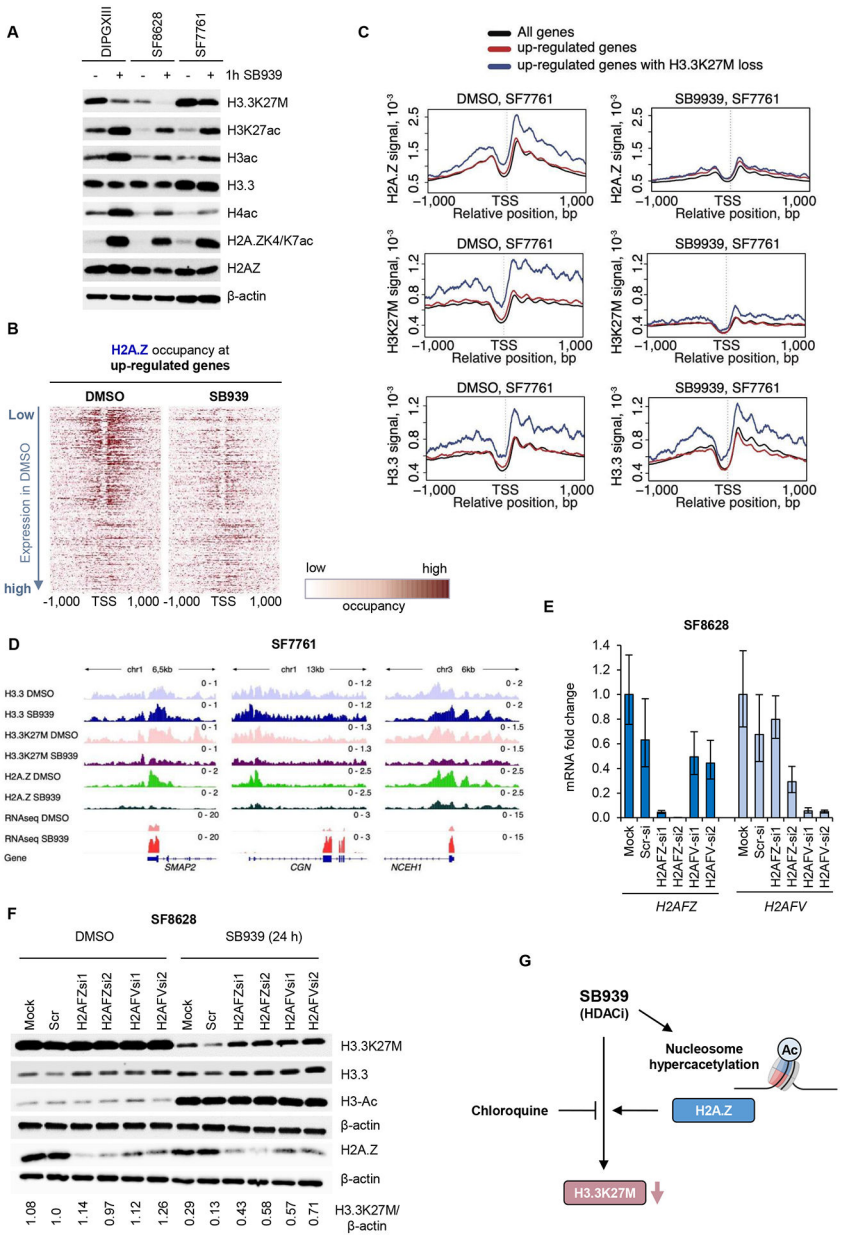

Figure 5. Presence of H2A.Z predisposes pHGG cells to the loss of H3.3K27M during HDAC inhibition with SB939.

A. DIPGXIII, SF8628 and SF7761 cells were exposed to 1 μM SB939 treatment for one hour and samples were subjected to Western blotting with the indicated antibodies. A representative blots of at least three independent experiments are shown.

B. Heatmaps showing the H2A.Z occupancy around transcriptional start sites (TSSs) in up-regulated genes in SF7761 cells. The left and right heatmap corresponds to DMSO and SB939 treatment, respectively. Rows in heatmaps were ordered by the gene expression level in control DMSO-treated cells (the lowest expression in DMSO at the top).

C. The histone variant profiles around TSS in SF7761 cells treated with SB939 for 16 hours. The average H2A.Z (top panel), H3.3K27M (middle panel) and H3.3 (bottom panel) profiles around TSS (+/−2kb) of all protein-coding genes (black line), all up-regulated genes (red),

and up-regulated genes with H3.3K27M loss after SB939 treatment (blue) are shown. The left and right plots correspond to control cells and cells after SB939 treatment, respectively.

D. Examples illustrating H3.3K27M and H2A.Z loss in SF7761 cells after SB939 treatment at up-regulated genes. Profiles of H3.3, H3.3K27M, H2A.Z ChIP-seq and RNA-seq at the loci encompassing selected up-regulated genes. Profiles were scaled for each gene locus individually.

E. SF8628 cells were double-transfected with siRNAs against *H2AFZ* and *H2AFV* transcripts, control siRNA (Scr-si) or Mock (no siRNA). Efficient knock-down of *H2AFZ* and *H2AFV* at 72 hours post-transfection was verified by qPCR with specific primers in relation to *GAPDH* housekeeping gene.

F. SF8628 cells were transfected as in **E** and 48 hours post-transfection cells were treated with 1 μM SB939 or DMSO for 24 hours. Samples were then subjected to Western blotting with the indicated antibodies. A representative experiment from three independent repeats is shown. The bottom panel shows quantitation of H3.3K27M densitometry normalised to β-actin.

G. A scheme showing SB939-dependent downregulation of H3.3K27M in DIPG cells. Upon treatment with SB939, histones present in the nucleosomes undergo rapid hyperacetylation, including the histone variant H2A.Z. Co-occurrence of H2A.Z predisposes cells to the SB939-mediated H3.3K27M loss. The loss of H3.3K27M by SB939 is blocked in the presence of chloroquine, a lysosomal inhibitor and DNA-intercalating agent.

Key resources table

REAGENT or RESOURCE	SOURCE	IDENTIFIER
Antibodies		
Anti-Histone H3 antibody - Nuclear Loading Control and ChIP Grade	Abcam	Cat# ab1791, RRID:AB_302613
Anti-Histone H3.3 antibody (*H3F3A*)	Millipore	Cat# 09–838, RRID:AB_10845793
Histone H3.3K27M antibody (pAb)	Active Motif	Cat# 61803, RRID:AB_2793773
Recombinant Anti-Histone H2A.Z antibody [EPR6171(2)(B)] - ChIP Grade	Abcam	Cat# ab150402, RRID:AB_2891240
Acetyl-Histone H2AZ (Lys4/Lys7) (D3V1I) Rabbit mAb	Cell Signaling Technology	Cat# 75336, RRID:AB_2799867
Anti-acetyl-Histone H3	Millipore	Cat# 06–599, RRID:AB_2115283
Acetyl-Histone H3 (Lys27) (D5E4) XP Rabbit mAb	Cell Signaling Technology	Cat# 8173, RRID:AB_10949503
Anti-acetyl-Histone H4	Millipore	Cat# 06–866, RRID:AB_310270
Cleaved Caspase-3 (Asp175) Antibody	Cell Signaling Technology	Cat# 9661, RRID:AB_2341188
Cleaved Caspase-7 (Asp198) Antibody	Cell Signaling Technology	Cat# 9491, RRID:AB_2068144
PARP Antibody	Cell Signaling Technology	Cat# 9542, RRID:AB_2160739
Anti-HDAC1	Millipore	Cat# 06–720, RRID:AB_2295297
Anti-HDAC2, clone 3F3	Millipore	Cat# 05–814, RRID:AB_310022
Monoclonal ANTI-FLAG® M2 antibody	Sigma-Aldrich	Cat# F3165, RRID:AB_259529
Anti-HIF-1 alpha antibody [EPR16897]	Abcam	Cat# ab179483, RRID:AB_2732807
Mouse Anti-Actin, beta Monoclonal Antibody, Horseradish Peroxidase Conjugated, Clone AC-15	Sigma-Aldrich	Cat# A3854, RRID:AB_262011
Anti-LC3B antibody produced in rabbit	Sigma-Aldrich	Cat# L7543, RRID:AB_796155
Chemicals, peptides, and recombinant proteins		
DMEM/F12	Gibco	Cat# 11330–032
N2 supplement	Cell Therapy Systems	Cat# A1370701
B27 Supplement w/o Vitamin A	Gibco	Cat# 12587–010
Recombinant human EGF	StemCell Technologies	Cat# 78006
Recombinant human bFGF	Miltenyi Biotec	Cat# 130-093-838
Recombinant human PDGF-AB	PeproTech	Cat# 100–00AB
Heparin	StemCell Technologies	Cat# 07980
poly-L-Ornithine	Sigma-Aldrich	Cat# P4957
Laminin 100X (EHS murine sarcoma)	Sigma-Aldrich	Cat# L2020
MEM Non-Essential Amino Acids	Gibco	Cat# 11140–050
Antibiotic-Antimycotic	Gibco	Cat# 15240–096
Penicillin-Streptomycin	Gibco	Cat# 15140122
MEM Sodium Pyruvate Solution 100 mM	Gibco	Cat# 11360–070
HEPES Buffer Solution (1M)	Gibco	Cat# 15630–080
GlutaMAX-I Supplement	Gibco	Cat# 35050–061

REAGENT or RESOURCE	SOURCE	IDENTIFIER
NeuroCult™ NS-A Proliferation Kit (Human)	StemCell Technologies	Cat# 05751
Neurobasal A	Gibco	Cat# 10888–022
Fetal Bovine Serum, qualified, heat inactivated	Gibco	Cat# 10500–064
Dynabeads™ Protein A	Invitrogen	Cat# 10001D
Proteinase K	Thermo Fisher Scientific	Cat# EO0492
Glycogen	Thermo Fisher Scientific	Cat# R0561
RNase A, DNase and protease-free	Thermo Fisher Scientific	Cat# EN0531
2× Fast SYBR GREEN PCR Master Mix	Applied Biosystems	Cat# 4385610
cOmplete™, EDTA-free Protease Inhibitor Cocktai	Sigma-Aldrich	Cat# 11873580001
SB939	Cayman	Cat# 15140122
Chloroquine	Sigma-Aldrich	Cat# C6628
MG-132	Sigma-Aldrich	Cat# 474787
Critical commercial assays		
jetPRIME transfection reagent	PolyPlus	Cat# 114–07
DharmaFECT 1 transfection reagent	Dharmacon	Cat# T-2001–02
Epigenetic Screening Library	Cayman	Cat# 11076
SuperScript™ III Reverse Transcriptase kit	Thermo Fisher Scientific	Cat# 18080093
Cell Proliferation ELISA, BrdU	Roche	Cat# 11647229001
RNeasy Plus Mini Kit	Qiagen	Cat# 74134
Deposited data		
RNA-seq and ChIP-seq sequencing raw and processed data	This paper	GSE232283
Mass Spectrometry data	This paper	MSV000093052
Experimental models: Cell lines		
SF8628 (DIPG; Pons; H3.3K27M, *H3F3A* mut)	Rintaro Hashizume's Lab, Northwestern University	N/A
SF7761 (DIPG; Pons; H3.3K27M, *H3F3A* mut)	Rintaro Hashizume's Lab, Northwestern University	N/A
SU-DIPGXIII parental and SU-DIPGXIII-KO$^{H3.3K27M}$ (DIPG; Pons; H3.3K27M, *H3F3A* mut)	Nada Jabado's Lab, McGill University	N/A
BT245 parental and BT245-KO$^{H3.3K27M}$ (GBM; Thalamus; H3.3K27M, *H3F3A* mut)	Nada Jabado's Lab, McGill University	N/A
HSJ019 parental and HSJ019-KO$^{H3.3K27M}$ (GBM; Thalamus; H3.3K27M, *H3F3A* mut)	Jacek Majewski's Lab, McGill University	N/A
CNHDMG-1008 (DIPG; Pons; H3.1K27M)	Javad Nazarian's Lab, Children's National Hospital,Washington, DC	N/A
CNHDMG-1277 (DIPG; Pons; H3.1K27M, *HIST1H3B* mut)	Javad Nazarian's Lab, Children's National Hospital,Washington, DC	N/A
7316–1769 (HGG; Cerebellum; H3.3K27M, *H3F3A* mut)	Children's Brain Tumor Tissue Consortium (CBTTC), The Children's Hospital of Philadelphia (CHOP)	7316–1769
7316–1763 (HGG; Thalamus; H3.3K27M, *H3F3A* mut)	CBTTC, CHOP	7316–1763

REAGENT or RESOURCE	SOURCE	IDENTIFIER
7316–195 (HGG; Cerebellum; H3.3K27M, *H3F3A* mut)	CBTTC, CHOP	7316–195
7316–913 (HGG; Temporal Lobe; H3 wild-type)	CBTTC, CHOP	7316–913
7316–1746 (HGG; Cerebellum; H3 wild-type)	CBTTC, CHOP	7316–1746
7316–85 (HGG; Temporal Lobe; H3 wild-type)	CBTTC, CHOP	7316–85
LN18 (Glioblastoma)	ATCC	Cat # CRL-2610
LN229 (Glioblastoma)	ATCC	Cat # CRL-2611
U-251 (other name U-373; Glioblastoma)	ATCC	Cat # HTB-17
Experimental models: Human patient biopsies		
DMG biopsy from the pons (H3.1K27M, *HIST1H3B* mut; female, 6 years); used to derive WG27 primary cells	This paper	N/A
DMG biopsy from the thalamus (H3.3K27M, *H3F3A* mut; male, 4 years); used to derive WG30 primary cells	This paper	N/A
DMG biopsy from the pons (H3.3K27M, *H3F3A* mut; male, 15 years); used to derive WG32 primary cells	This paper	N/A
Oligonucleotides		
NTC-control siRNA: CUCUCGCUUGGGCGAGAGUAAGtt	Eurofins	N/A
H2AFZ-si1 siRNA: CCGUAUUCAUCGACACCUAtt	Eurofins	N/A
H2AFZ-si2 siRNA: GACUUAAAGGUAAAGCGUAtt	Eurofins	N/A
H2AFV-si1 siRNA: GCAGUAUCUCGCUCACAGAtt	Eurofins	N/A
H2AFV-si2 siRNA: CAGGUAAUGCUUCUAAGGAUCUCAA	Eurofins	N/A
ON-TARGETplus Human HDAC1 (3065) siRNA	Dharmacon	L-003493-00-0020
ON-TARGETplus Human HDAC2(3066) siRNA	Dharmacon	L-003495-02-0020
Flag-H3.3K27M mutagenesis forward primer GAGTGCGCCCTCTACTGG	Genomed	N/A
Flag-H3.3K27M mutagenesis reverse primer ATGCGAGCGGCTTTTGTAG	Genomed	N/A
Primers for RT-PCR	Genomed	Table S2
Recombinant DNA		
pcDNA4/TO-Flag-H3.3	Huang et al., 2013 [44]	Gift from Bing Zhu, Cat#47980; RRID:Addgene_47980
pcDNA4/TO-Flag-H3.3K27M	This paper	N/A
Software and algorithms		
R/Bioconductor	https://www.r-project.org/	N/A
Tophat	https://ccb.jhu.edu/software/tophat/index.shtml	N/A
HTseq	https://htseq.readthedocs.io/en/release_0.11.1/index.html	N/A
samtools	http://www.htslib.org/	N/A
bowtie	https://bowtie-bio.sourceforge.net/index.shtml	N/A
MACS	https://github.com/macs3-project/MACS/tree/macs_v2	N/A
EpiProfile	https://github.com/zfyuan/EpiProfile2.0_Family	N/A

REAGENT or RESOURCE	SOURCE	IDENTIFIER
Skyline	https://skyline.ms/project/home/software/Skyline/begin.view	N/A